Neurological mechanism of sensory deficits after developmental exposure to non-dioxin-like polychlorinated biphenyls (PCBs)

Nadja R. Brun[1], Jennifer M. Panlilio[1], Kun Zhang[2,3], Yanbin Zhao[2,3], Evgeny Ivashkin[4,5], John J. Stegeman[1], Jared V. Goldstone[1]

[1] Department of Biology, Woods Hole Oceanographic Institution, Woods Hole, MA, USA
[2] School of Environmental Science and Engineering, Shanghai Jiao Tong University, 800 Dongchuan Road, Shanghai 200240, China
[3] Shanghai Institute of Pollution Control and Ecological Security, Shanghai 200092, China
[4] Josephine Bay Paul Center for Comparative Molecular Biology and Evolution, Marine Biological Laboratory, Woods Hole, MA, USA
[5] A.N. Severtsov Institute of Ecology and Evolution, Russian Academy of Sciences, Moscow, Russia

Address correspondence to Nadja Brun: nbrun@whoi.edu

Abstract

The most abundant polychlorinated biphenyl (PCB) congeners found in the environment and in humans are the *ortho*-substituted, non-dioxin-like (NDL) congeners, especially PCB153. While evidence indicates that exposure to PCB153 and other NDL-PCBs in early vertebrate development can contribute to neurobehavioral disorders, the basis of neurobiological effects of NDL-PCBs is poorly understood. We assessed a range of effects of several NDL-PCB congeners (PCB153, PCB52, PCB118, and PCB138) on synaptic transmission and cellular morphologies linked to the proper execution of a sensorimotor response in zebrafish, taking advantage of the well-established neural circuit in this model. Startle responses were dramatically delayed in 6-day old larvae exposed to NDL-PCB. In contrast, exposure to the dioxin-like PCB126 did not delay startle response times. Morphological and biochemical data showed that exposure to NDL-PCBs during development induces swelling of afferent sensory neurons and disrupts dopaminergic and GABAergic signaling associated with motor movement. This study demonstrates that connections between neurotoxic mechanisms and processing of sensory stimuli occur at low concentrations of NDL-PCBs, similar to those present in human and animal samples. The effects on important and broadly conserved signaling mechanisms in vertebrates suggest that NDL-PCBs can contribute to neurodevelopmental abnormalities, relevant for both exposed human populations and wildlife.

Keywords

Developmental neurotoxicology, motor behavior, PCB153, startle response, zebrafish

35 # 1 Introduction

36 Humans and wildlife are exposed to a wide range of contaminants in the environment, and the
37 role of these chemical pollutants in developmental neurotoxicity, cognitive impairment, and
38 neurodegenerative disorders has become a global environmental health concern (Landrigan et
39 al., 2018). Among the top industrial chemicals thought to be involved in developmental
40 neurotoxicity are polychlorinated biphenyls (PCBs) (Grandjean and Landrigan, 2014), a mix of
41 209 different structures, including planar dioxin-like (DL) congeners and non-planar non-dioxin-
42 like (NDL) congeners. PCBs are persistent legacy contaminants that have been produced and
43 used for decades to serve as insulators, coatings, and caulks, and there is worldwide PCB
44 contamination of wildlife tissue and human cord blood, amniotic fluid, and mother's milk
45 (Ennaceur et al., 2008; Lancz et al., 2015a). The developing nervous system is generally
46 sensitive to chemical exposure at doses much lower than those affecting adult nervous system
47 function (Rice and Barone, 2000). For instance, prenatal exposure to PCBs is associated with a
48 decrease in motor skills in infants, while postnatal exposure seems to have no obvious effects
49 (Ribas-Fitó et al., 2001). Thus, identifying the mechanisms underpinning the effects of
50 neurotoxic PCBs during gestation and early life stages is of critical importance in attaining
51 successful treatments and remediating health effects in humans and wildlife due to
52 environmental exposure.

53 The NDL-PCBs are the most abundant congeners in human and environmental samples. The
54 NDL-PCB138 and PCB153, are particularly abundant. Median PCB153 concentrations
55 measured in human cord blood serum range from 6.4 to 110 ng g^{-1} lipid (Bergonzi et al., 2009;
56 Herbstman et al., 2007; Lancz et al., 2015b), far greater than the levels of DL congeners.
57 Evidence also suggests the NDL-PCBs contribute substantially to neurotoxic and behavioral
58 effects (Boix et al., 2010; Boucher et al., 2009). However, understanding of the mechanisms

59 and effects of NDL-PCBs, especially during the more sensitive early stages of development,
60 significantly lags that of DL-PCBs.

61 Increased serum PCB concentrations in children are associated with deficits in cochlear
62 functions (Jusko et al., 2014; Trnovec et al., 2010), fine motor skills (Walkowiak et al., 2001),
63 and cognitive impairment (Boucher et al., 2009; Chen et al., 1992). Developmental exposure of
64 animals to NDL-PCBs has been linked to behavioral changes, including hyperactivity,
65 impulsiveness, and impairment of cognitive function (e.g., impairment of the ability to learn the Y
66 maze task) (Berger et al., 2001; Johansen et al., 2014; Schantz et al., 2003). NDL-PCB
67 developmental exposure also adversely affects auditory function in adult rats, including elevated
68 thresholds of brainstem auditory evoked potentials, auditory deficits at low frequencies,
69 audiogenic seizures, and reduced auditory startle responses (Crofton et al., 2000; Goldey et al.,
70 1995; Lilienthal et al., 2015, 2011; Poon et al., 2015). The mechanism(s) involved in these
71 effects on cognitive and auditory systems are not known.

72 Zebrafish are increasingly used as model organism to uncover the mechanisms of neurotoxicity
73 that are relevant for humans and other vertebrates. Zebrafish remain transparent throughout
74 early development, facilitating the use of transgenic and other molecular approaches to label
75 and observe specific classes of neurons and to follow their functional development. Fish have
76 relatively simple neural circuits, particularly for the auditory system. In fish, the auditory-evoked
77 startle response plays a critical role in animal survival, and involves cellular functions, sensory-
78 motor pathways, and monoamine neurotransmitters that are conserved among vertebrates
79 (Stewart et al., 2014). Many of the pathways and genes that regulate zebrafish startle behavior
80 also operate in human neurological disorders (Howe et al., 2013; Maximino and Herculano,
81 2010; Meserve et al., 2020; Tropepe and Sive, 2003; Wolman et al., 2015). In this study, we use
82 the zebrafish startle response to decipher the neuro-disruptive basis of NDL-PCBs on the
83 auditory system during the early stages of development. To this end, we examined the effects of

84 different NDL-PCBs (PCB153, PCB52, PCB118, PCB138), in comparison to the DL-PCB126
85 and at different environmentally relevant concentrations, dissecting various steps in the neural
86 circuitry underlying the acoustic startle response.

87 # 2 Materials and Methods

88 ## 2.1 Animal model

89 In addition to other attributes, zebrafish have relatively simple neural circuits, particularly for the
90 auditory system. Many of the components of the auditory circuit are homologous in mammals
91 and fish, including hair cells, neural transmission, and lower motorneurons, while the
92 mechanosensory lateral line system and Mauthner (M) cells are exclusively found in fish and a
93 cochlea is only found in mammals. In fish, vibro-acoustic stimuli are first sensed by the hair cell
94 bundles in the auditory, vestibular, and lateral-line systems and rapidly encoded into trains of
95 action potentials in the afferent neurons (**Figure 1**) (Hudspeth, 1985). The signal detected
96 through the sensory hair cells of the lateral line is transmitted through the anterior and posterior
97 lateral line ganglia whereas the auditory input is transmitted through the VIIIth statoacoustic
98 nerve, all of which synapse to the lateral dendrite of the M-cell and two segmental homologs
99 (Nakayama, 2004; Pujol-Martí and López-Schier, 2013). The signal is propagated down the M-
100 cell axon in the spinal cord to activate the motoneurons leading to a unilateral contraction of the
101 trunk musculature.

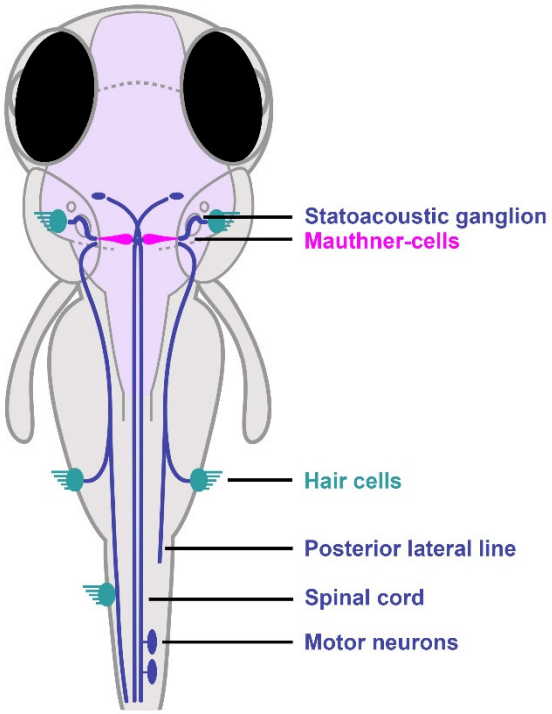

Figure 1. Startle response circuit in zebrafish. The proper execution of the startle response relies on hair cells to sense the auditory stimulus, Mauthner-cells to integrate the signals, and motor neurons and musculature to execute the startle behavior.

2.2 Zebrafish husbandry and early-life stage exposure

Zebrafish (*Danio rerio*) were maintained at 28.5 °C and on a 12:12 h light-dark cycle according to the guidelines of the Zebrafish Model Organism Database (ZFIN, http://zfin.org) and institutional guidelines at WHOI and the experimental procedures approved by the Institutional Animal Care and Use Committee (ID Number BI21981.01). Adult zebrafish were fed brine shrimp and pellets every day. In this study, we used wild-type zebrafish of the AB strain obtained from Zebrafish International Resource Center (ZIRC), as well as several transgenic lines: the photoconvertible calcium indicator line *Tg[elavl3:CaMPARI(W391F+V398L)]*^{jf9} kindly provided by Jessica Plavicki (Brown University, USA), and the transgenic lines *Tg(cntn1b:EGFP-CAAX)* (Panlilio et al., 2021) labeling axons, *Tg(olig2:EGFP)*^{vu12} (Park et al., 2007; Shin et al., 2003) marking oligodendrocyte precursor cell bodies, *Tg(sox10:mRFP)*

117 (Takada et al., 2010) marking oligodendrocyte lineage cells, as well as *Tg(mbp:EGFP-CAAX)*
118 (Almeida et al., 2011) *and Tg(mbp:EGFP)* (gift from Dr. Kelly Monk, generated by Dr. Charles
119 Kaufman in the laboratory of Dr. Leonard Zon, Harvard Medical School, Boston, MA) marking
120 myelin sheaths. Zebrafish eggs were obtained by pairwise breeding and kept in 0.3x Danieau's
121 (17 mM NaCl, 0.2 mM KCl, 0.12 mM $MgSO_4$, 0.18 mM $Ca(NO_3)_2$ and 1.5 mM HEPES, pH 7.6)
122 in glass vials at a density of 10 individuals per 10 mL, at a constant water temperature of 28 ±
123 1˚C and standard 14-h light/10-h dark cycle. The medium was supplemented with 1-Phenyl-2-
124 thiourea (PTU, 0.003% w/v) from 24 hours post-fertilization (hpf) onwards to prevent pigment
125 formation when necessary for imaging. Fertilized eggs were used for exposures starting at 3 hpf
126 to solvent control (0.1% DMSO, v/v), 2,2′,4,4′,5,5′-hexachlorobiphenyl (PCB153), 2,2′,5,5′-PCB,
127 2,2′,5,5′-tetrachlorobiphenyl (PCB52), 2,3',4,4',5-pentachlorobiphenyl (PCB118), 2,2',3,4,4',5'-
128 hexachlorobiphenyl (PCB138), or 3,3',4,4',5-hexachlorobiphenyl (PCB126). Additionally, one
129 exposure scenario with PCB153 was started at 24 hpf, to assess whether effects are induced
130 during or after initial neuronal cell differentiation. Sensory neurons send their projection along
131 the ectoderm as early as 16 hpf (Kimmel, 1993). The lowest exposure concentration for
132 PCB153 was 10 nM (3.6 ng mL^{-1}) which is estimated to result in ~5 ng g^{-1} (5 ppm) per zebrafish
133 larvae (comparing to PCB95 uptake levels; (Ranasinghe et al., 2019)). PCB153 mean
134 concentrations found in maternal cord blood serum are 0.27 ng mL^{-1} or 110 ng g^{-1} lipid (Lancz et
135 al., 2015b)). Other concentrations used were 30, 100, and 1000 nM which are found in fish of
136 contaminated ecosystems (Gräns et al., 2015). For PCB52, PCB118, and PCB138, a
137 concentration of 1000 nM was chosen to compare to the highest effect concentration of
138 PCB153. The DL-PCB126 is cardioteratogenic in the low nanomolar range. To avoid
139 malformations, a concentration of 1 nM was chosen. Exposures were refreshed daily until four
140 days post-fertilization (dpf) and all larvae were kept in Danieau's from 5 to 6 dpf. All imaging and
141 behavioral assays were performed at 6 dpf, except for the touch assay, which was performed at
142 26 hpf.

143 The influence of neurotransmitters on the startle behavior was assessed by exposures to
144 compounds known to interfere with monoamines. At 6 dpf, larvae were evaluated for their startle
145 behavior and then immersed in the dopamine precursors L-DOPA (1 mM) or L-tyrosine (1 mM),
146 dopamine receptor agonist quinpirole (10 μM), dopamine D2-receptor antagonist and GABA
147 receptor modulator haloperidol (10 μM), endogenous serotonin 5-HT (10 μM), and serotonin
148 precursor 5-HTP (1 mM) for 30 min in the well plate before assessing the startle behavior again.
149 Additionally, the effect of neurotransmitter modulation during development on startle response
150 was assessed by exposing larvae from 3 to 120 hpf to L-DOPA (1 mM), L-tyrosine (1 mM), and
151 quinpirole (10 μM).

152 **2.3 Behavioral Analysis**

153 Larval locomotion was monitored using the Noldus Daniovison system (Noldus Information
154 Technology, Leesburg, VA, USA) using 6-dpf larvae distributed in 48-well plates (1 larva per
155 well). After an acclimation period of 40 minutes in the illuminated chamber, spontaneous
156 swimming activity was tracked for 10 minutes. Following the spontaneous swimming, three
157 alternating cycles of dark and light conditions (10 minutes each) were run. The experiment was
158 repeated three times with cohorts from separate breeding events (*n* = 24 per group and
159 breeding event). Video data were recorded with 30 frames per second via an infrared camera.
160 Obtained data were analyzed with the supplied software EthoVision XT® 12 (Noldus. Inc.).

161 The activity of Rohon-Beard sensory neurons was tested at 26 hpf by lightly touching DMSO-
162 and 1000 nM PCB153-exposed embryos (*n* = 10 per group and breeding event) using a piece of
163 fishing line affixed to a glass pipette. Each embryo was touched ten times and the response was
164 scored as follows: 0, no response; 0.5, light tail flicking response, 1, coiling in the opposite
165 direction of the touch stimulus, yielding a score of maximum 10 per embryo. The experiment
166 was repeated twice with cohorts from separate breeding events.

167 Vibro-acoustic startle response was assessed as described previously (Panlilio et al., 2021).
168 Briefly, the acoustic stimuli were delivered by a vibrational exciter producing acoustic vibrations
169 at a frequency of a 1000 Hz for a duration of 2 ms at four different amplitudes (32, 38, 41, 43
170 dB). For each amplitude, the stimulus was delivered four times, spaced 20 seconds apart, to a 4
171 x 4 well-plate mounted on top of the speaker, each well containing an individual larva. The
172 response was tracked with a high-speed camera (Edgertronic SC1) at 1000 frames s^{-1} for 250
173 ms (13 ms before and 237 ms after the stimulus). PulsePal was used to synchronize the camera
174 recording to the acoustic stimuli using a TTL pulse. Automated analysis of larval movement
175 kinematics (response frequency, latency, turning angle) was performed using the FLOTE
176 software package (Burgess and Granato, 2007). Each treatment group was assessed at least
177 three times with eggs from different clutches. The total replicate numbers are stated in the
178 **Table S1 (Supplemental Material)**.

179 A startle response in fish can be executed with a short latency C-bend (SLC) or long latency C-
180 bend (LLC), with the SLC being the more frequent response at higher stimulus intensities. The
181 cut-off time between SLC and LLC can vary depending on environmental conditions such as
182 temperature and has been determined empirically for this experiment using a Gaussian mixture
183 model (Panlilio et al., 2020)(**Figure S1**). Responses within 15 ms were categorized as SLC,
184 latencies greater than 15 ms as LLC. Following this classification, the median response type
185 (Relative Startle Bias) for each responsive fish was determined for each stimulus intensity (32,
186 38, 41, and 43 dB). Bias per individual fish was calculated as: (frequency of SLC – frequency of
187 LLC) / total responses. Pure SLC responses result in a value of +1, while pure LLC responses
188 are a value of -1 (Jain et al., 2018).

189 Electric field pulses (EFPs) directly activate the M-cells (Tabor et al., 2014). Responsiveness of
190 M-cells was assessed by applying EFPs (4.4 V cm^{-1} for 2 ms, square pulse) to head-restrained
191 larvae (*n* = 46 per treatment group). Seven consecutive EFPs were applied with a recovery time

192 of 20 s in between pulses. For each run, one control and one exposed larva were embedded in
193 1.5% agarose side-by-side and their tails freed. Response frequency, latency, and bend angle
194 were tracked using FLOTE. For all behavioral assays, only larvae with an inflated swim bladder
195 were used.

196 **2.4 Larval growth**

197 Larval length (from snout to the tail-fin end) was measured in DMSO (*n* = 57) and 1000 nM
198 PCB153 (*n* = 51) exposed larvae using ImageJ. The experiment was performed three times with
199 embryos from different clutches.

200 **2.5 FM1-43 labeling**

201 The vital fluorescent dye FM1-43 (n-(3-triethylammoniumpropyl)-4-(4-(dibutylamino)-styryl)
202 pyridinium dibromide; Invitrogen) specifically labels hair cells in the lateral line and inner ear of
203 vertebrates of by entering through open mechanotransduction channels and filling the
204 cytoplasm of hair cells (Meyers et al., 2003). At 6 dpf, zebrafish larvae of 1000 nM PCB153-
205 exposed (*n* = 32) and unexposed (*n* = 28) groups were immersed in Danieau's supplemented
206 with 3 μM FM1-43 for 30 s, rinsed three times in Danieau's, anesthetized in 1 mM 3-amino-
207 benzoic acid (Tricaine), and mounted in 1.5% low melting agarose for confocal imaging of the
208 L3 neuromast. The experiment was performed three times independently.

209 **2.6 Immunohistochemistry**

210 Whole-mount immunohistochemistry of zebrafish larvae and brains was performed following
211 standard procedures. Briefly, 10 AB larvae per exposure group were treated as described above
212 and subsequently fixed in 4% paraformaldehyde (PFA) in PBS overnight at 4 ˚C. For labelling
213 brain tissue, larval brains were dissected before continuing with the protocol. Multiple rinsing
214 steps in PBS containing either 0.5% Triton-X100 or 0.1% Tween-20 (PBST) for larvae or brains,
215 respectively, was followed by an antigen retrieval step in 150 mM Tris HCl (pH 9.0) at 70 °C

216 (Inoue and Wittbrodt, 2011), and a permeabilization step using proteinase K (10 µg/mL for 3
217 minutes). Subsequently, the samples were blocked in blocking solution (10% Normal Goat
218 Serum, 1% DMSO, 1% BSA, 88% PBST) for 1 h and then stained with blocking solution
219 supplemented with the primary antibody for three days at 4 ˚C. The primary anti-neurofilament
220 mouse polyclonal antibody (3A10; Developmental Hybridoma Bank, 1:100 dilution) was used to
221 label a subset of hindbrain spinal cord projecting neurons such as the M-cell neurons (DMSO *n*
222 = 23, PCB153 *n* = 21). The anti-5HT rabbit polyclonal antibody (Sigma-Aldrich, #S5545, 1:500)
223 was used to label serotonergic cells (DMSO *n* = 16, PCB153 *n* = 13). The anti-acetylated alpha-
224 tubulin mouse polyclonal antibody (Sigma-Aldrich, #T6793, 1:1000 dilution) was used to label
225 kinocilia and hair cell innervating neurons (DMSO *n* = 25, PCB153 *n* = 24). After several
226 washing steps, in PBST, the samples were incubated with Alexa Fluor 488- or 594-conjugated
227 goat-anti-mouse or goat-anti-rabbit secondary antibodies (Abcam, 1:500 dilution) overnight at 4
228 ˚C and rinsed several times in PBST before mounting in ProLong Diamond Antifade mountant
229 (Invitrogen) for imaging. For visualization of skeletal muscle fibers (DMSO *n* = 11, PCB153 *n* =
230 11), larvae were fixed as above, followed by permeabilization in 5% Triton-X for overnight and
231 incubation in phalloidin Alexa-546 conjugate (Invitrogen, 1:500). All staining experiments were
232 repeated three times with larvae from independent clutches except the phalloidin staining, which
233 were performed once.

234 2.7 Formation of hair cell innervating neurons, primary motoneuron, and 235 oligodendrocyte lineage cells

236 The *Tg(cntn1b:EGFP-CAAX)* transgenic line was used to image the cell bodies of neurons that
237 innervate the hair cells at the L3 position in the lateral line (DMSO *n* = 22, PCB153 *n* = 20, two
238 independent experiments). The axons of the main caudal primary motoneurons were visualized
239 using the *Tg(olig2:EGFP)* transgenic line (*n* = 4 per treatment group, one experiment). The
240 double transgenic *Tg(olig2:EGFP) x Tg(sox10:mRFP)* was used to quantify oligodendrocyte

241 lineage cells in the spinal cord of in DMSO (*n* = 22) and 1000 nM PCB153 (*n* = 16) treated
242 larvae (Shin et al., 2003). All larvae were anesthetized in tricaine (0.16% MS222) before
243 mounting laterally in 1.5% low melting agarose on a glass-bottom microscopy dish (MatTek).
244 Fluorescently labelled cell bodies were imaged at the distal end of the intestine, around the L3
245 neuromast. The experiments were performed three times independently.

246 **2.8 Calcium imaging of freely swimming and startling larvae**

247 Neuronal activity in DMSO- and PCB153-treated larvae was visualized using the CaMPARI
248 (*elavl3*:CaMPARI) transgenic zebrafish line with an engineered fluorescent protein that
249 permanently photoconverts from green to red in the presence of elevated calcium and UV light
250 (Fosque et al., 2015). Photoconversion was achieved by mounting an LED light (405 nm;
251 LEDSupply) between the speaker and a custom-made 3-well plate containing the freely
252 swimming larvae (DMSO- and PCB153-treated). Larvae of the same treatment were divided into
253 two batches: one was photoconverted in medium at room temperature (RT) and the other one at
254 4˚C to elicit high neuronal activity. Photoconversion was achieved by shining the LED light for
255 10 sec either with one vibrational stimulus of 43 dB at the start or without stimulus.
256 Subsequently, larvae were anesthetized, embedded in agarose, and whole brains imaged using
257 the 10x objective. The experiment was performed twice (*n* = 11-16 per treatment group).

258 **2.9 Image processing**

259 Whole-brain, hair cells, M-cell, and motor neurons were imaged on a Zeiss LSM 800 confocal
260 system with a 10x/0.45 Plan-Apochromat, 20x/0.8 Plan-Apochromat, or 63x/1.2 C-Apochromat
261 water immersion objective. Airy scan was applied for hair cell imaging at 63x. Z-stacks were
262 merged to a single plane by maximal intensity projection using Fiji (Schindelin et al., 2012). The
263 number of *olig2* cells dorsal of the spinal cord (DMSO *n* = 22, 1000 nM PCB153 *n* = 16) was
264 counted in confocal image stacks using the 3D projection of the Zeiss Zen blue software.

265 Myelination was evaluated after imaging the spinal cord (DMSO *n* = 26, 1000 nM PCB153 *n* =
266 27) using the 20x objective and scored for deficits according to Panlilio et al. 2020.
267 Representative myelination was imaged at 40x. The intensity of serotonergic neurons in the
268 brain (DMSO *n* = 16, 1000 nM PCB153 *n* = 13) was measured performing a Sum Slices Z-
269 projection followed by drawing a ROI around the 5-HT immuno-responsive cells, and per image,
270 three random squares (area size = 10.65 x 10.65) within the non-fluorescent area of the ROI for
271 background subtraction (for orientation see **Figure S12**). Similarly, the FM1-43 intensity was
272 measured drawing a ROI around the fluorescent hair cells and measuring the background in
273 three random squares (DMSO *n* = 20, 1000 nM PCB153 *n* = 20). Corrected total cell
274 fluorescence (CTCF) was calculated according to the formula: Integrated density - (ROI x Mean
275 fluorescence of background readings). For quantification of active neurons in the brain of freely
276 swimming and startling CaMPARI zebrafish larvae, Sum Slices Z-projection were analyzed for
277 red fluorescence intensity in the rostral hindbrain (for orientation see **Figure S13**).

278 The volume of hair cell innervating neurons was calculated by measuring the volume of
279 thresholded pixels (30-255, Otsu method) in image stacks using an imageJ macro looping
280 through the stack and summing the area measurements, then multiplying this sum by the depth
281 of each slice (DMSO *n* = 30, 1000 nM PCB153 *n* = 29). The presence of primary motor neurons
282 was confirmed using the Simple Neurite Tracer plugin in Fiji (DMSO *n* = 21, 1000 nM PCB153 *n*
283 = 18). All image evaluations and quantifications were done without the knowledge of the
284 experimental condition of the specimens.

285 **2.10 Neurotransmitter analysis**

286 The analysis of neurotransmitters, including histamine, L-histidine, L-glutamic acid, gamma-
287 aminobutyric acid (GABA), acetylcholine, L-DOPA, 3-methoxytyramine, serotonin, 5-
288 hydroxyindole-3-acetic acid, glycine, L-glutamine, L-valine, 3-hydroxytyramine and choline, was
289 performed with a method developed in a previous study (Zhao et al., 2020). Briefly, the

290 zebrafish embryo samples were spiked with 100 ppb isotope-labeled internal standards and
291 then homogenized. The homogenized tissue samples were extracted with 200 μL of 80:20 v/v
292 ACN/Milli-Q water containing 0.1% formic acid and 1% ascorbic acid and 200 μL ACN. After
293 protein precipitation, the supernatants were dried and redissolved in 100 μL of Milli-Q water
294 containing 0.1% formic acid for UHPLC-MS/MS analysis. Neurotransmitters were quantified by
295 a high-performance liquid chromatography system coupled to a Q-Exactive plus quadrupole-
296 Orbitrap mass spectrometer (UHPLC-Q-Orbitrap, Thermo fisher, US). The separation of
297 neurotransmitters was carried out by an Acquity UPLC HSS T3 column with Milli-Q water
298 containing 0.1% formic acid and ACN containing 0.1% formic acid as mobile phase. The MS
299 acquisition was performed in the full scan mode and parallel reaction monitoring mode. The
300 experiment was performed once (*n* = 4 per treatment group).

301 **2.11 Statistical Analyses**

302 All statistical analyses were conducted using Graph Pad Prism 8.4 except some of the startle
303 behavior analysis, which was completed in R. All quantitative data were tested for normality
304 using the Shapiro-Wilk test, and if there were unequal number of subjects between groups, the
305 data were tested for homogeneity in variances using the Brown-Forsythe test. All treatment
306 groups were compared to respective control groups.

307 Responsiveness to auditory stimuli (response or not) and startle type (SLC vs. LLC) was
308 modelled in R (version 4.0.2) using a binomial generalized linear mixed effect model (glmer()
309 from the lme4 R package) (Bates et al., 2015). The response to electrical stimulus was modeled
310 using glm() from the lme4 R package. For the auditory response, we included treatment as a
311 fixed effect and the replicate experimental trials as a random effect. The model specification for
312 “fraction responding” was as follows: Responders ~ TreatmentGroup + (TreatmentGroup|trial).
313 The model specification for “startle bias” was as follows: SLCorLLCresponse ~ TreatmentGroup

314 + stimdB + (1|trial). The data were analyzed fitting the model for each stimulus intensity
315 independently. The model specification for the electrical stimulation are as follows: Responders
316 ~ TreatmentGroup.

317 To assess treatment differences of normal data with three or more groups (fluorescence
318 intensity CaMPARI), ANOVA comparisons were performed followed by a multiple comparison
319 using the Tukey's correction to adjust the critical values. A Tukey-corrected *p*-value < .05 was
320 considered statistically significant. For normal data with heterogeneity within-group variances
321 (LLC bend angle), a Welch ANOVA followed by a Dunnett's T3 multiple comparison test was
322 performed. For non-normal data with three or more groups (SLC bend angle), a Kruskal-Wallis
323 followed by the Dunn's multiple comparison test was performed. For normal data with two
324 groups (length, mean latency, bend angle in e-stim, oligodendrocyte lineage cell count, 5-HT
325 intensity), an unpaired two-tailed t-test with Welch's correction (Welch's t- test) was performed.
326 The nonparametric scoring data of the touch assay and latency in e-stim was analyzed using a
327 two-tailed Mann-Whitney test. The data are presented as mean ± *SD* with single data points
328 (replicates) superimposed on the graph unless specified in the figure legend.

329 3 Results

330 The startle response circuit is of wide relevance and well-established for assessing the influence
331 of specific factors on neuronal cell development, neuromuscular connectivity, and transmission
332 (Burgess and Granato, 2007; Medan and Preuss, 2014; Meserve et al., 2020; Panlilio et al.,
333 2020). We used the startle response circuit to assess the effects of NDL-PCBs on the formation
334 of neuronal populations and neurotransmission and its consequences for mechanosensory
335 disruptions, thus encompassing hearing and touch.

336 ### 3.1 Behavioral effects

337 Rohon-Beard cells are the earliest mechanosensory neurons that develop. They are located in
338 the dorsal region of the embryonic spinal cord and appear around 24 hpf (Roberts, 2000). A few
339 days into development, Rohon-Beard cells also relay sensory information to the M-cells (Liu and
340 Hale, 2017). In our experiments, a tactile stimulus on the trunk at 26 hpf evoked a C-shaped
341 body flexion in both the DMSO- and the 1000 nM PCB153-treated embryos (U = 183, p = .599;
342 **Figure S2**), indicating that the formation and function of Rohon-Beard cells were not impaired
343 by PCB153.

344 Exposure to contaminants during development can result in reduced growth, which can affect
345 kinematics in swimming behavior (Voesenek et al., 2018). PCB153-exposed larvae developed
346 normally with no difference in body length on day six in comparison to the control group, in all
347 three trials (Trial 1: $t(25.98) = .661$, $p = .514$; Trial 2: $t(37.98) = .443$, $p = .660$; Trial 3: $t(37.43) =$
348 $.645$, $p = .523$; **Figure S3**). At 6 dpf, spontaneous and light-dark-stimulated swimming activity
349 was assessed. Larvae exposed to PCB 153 (1000 nM) had lower cumulative locomotion activity
350 over ten minutes (M = 1182 mm, SD = 382) in comparison to the control group (M = 1510 mm,
351 SD = 402), $t(132.4) = 4.854$, $p < .0001$ (**Figure S4A**). Zebrafish larvae typically increase
352 locomotion in dark conditions following light exposure. Once stimulated with a rapid loss of
353 illumination during the dark phase, both treatment groups exhibited similar swimming activity
354 (**Figure S4B**).

355 The vibro-acoustic startle response can be executed either rapidly, within 15 ms (short latency
356 C-bend; SLC), or beginning at longer times and extending for up to 100 ms (long latency C-
357 bend; LLC). The mean latency value, representing the population response including SLC and
358 LLC responses, was 21 ± 20 ms for control larvae at the highest stimulus intensity (**Figure S1**,
359 **Figure 2A, B**). By contrast, the NDL-PCB-treated larvae that responded to the vibro-acoustic
360 stimulus showed significantly longer average latencies in response to the same auditory

361 stimulus given the controls, $F(5, 907 = 14.61$, $p < .0001$). PCB153-treated (1000 nM) larvae
362 responded at a mean latency of 68 ± 32 ms, PCB138 at 52 ± 37 ms, PCB118 at 45 ± 27 ms,
363 and PCB52 at 39 ± 32 ms. For PCB153, a dose-dependent response was observed, with mean
364 latencies increasing with dose (10 nM: 26 ± 27 ms, 30 nM: 50 ± 36 ms, 100 nM: 50 ± 30 ms,
365 1000 nM: 68 ± 32 ms). The lowest PCB153 concentration tested (10 nM) was not significantly
366 different from controls. Unlike NDL-PCB treated larvae, the DL-PCB126-treated larvae had a
367 mean latency (22 ± 22 ms), which was not significantly different from controls.

368 Examining the SLC and LLC responses separately can give insight into the underlying
369 mechanism of effect. A greater stimulus intensity increases the probability of evoking SLC,
370 shifting the response bias from LLC to SLC (Troconis et al., 2017). Here, we also observed a
371 shift to SLC with increasing stimulus intensity in solvent control (DMSO-treated) larvae (**Figure
372 2C, Figure S5A**). Larvae were tested four times at each stimulus intensity; thus, a larva is
373 categorized as having SLC bias if it responded 3 or 4 times out of 4 stimuli with an SLC. At the
374 highest stimulus intensity that we tested (43 dB), the majority of control larvae (300/448)
375 responded with a SLC within 7 ± 3 ms. 43 larvae showed no bias towards SLC or LLC (2 times
376 SLC and 2 times LLC, bias = 0). Those that did not perform an SLC (n = 105) exhibited an LLC
377 with a mean latency of 54 ± 29 ms (**Figure 2C**). In contrast, all NDL-PCB-treated larvae (except
378 for 10 nM PCB153) retained a response bias towards LLC at all stimulus intensities tested,
379 which was significantly different from the control ($p < .001$ for all stimulus intensities). Lowering
380 the PCB153 dose gradually increased the shift towards SLC, yet 10 nM PCB153 was still
381 significantly different from the control ($p < .01$ for all stimulus intensities). Exposures starting
382 after many structures of the brain and the neural tube have developed, at 24 hpf (Smith and
383 Kimelman, 2019), had the same effect on startle latency (**Figure S5B)**.

384 The proportion of control larvae responding to the stimulus (either SLC or LLC) increased from
385 75.2 ± 33.0% (n = 450) to 95.8 ± 17.0% (n = 457) from the lowest to highest stimulus intensity,

386 whereas the proportion of NDL-PCB153-, PCB138-, and PCB52-treated larvae that responded
387 remained below 70% (except for 10 nM PCB153) at all intensities and were significantly
388 different ($p < .01$) from the control (**Figure 2D**, **Figure S6A**). In contrast to those exposed to
389 NDL-PCBs, the larvae exposed to the DL-PCB126 and NDL-PCB118 had a response latency
390 and rate similar to the control larvae.

391 The different startle response bends exhibit different kinematics, with SLCs exhibiting larger
392 bend angles and faster angular velocities than LLCs (Burgess and Granato, 2007). Thus, LLC
393 and SLC kinematics were analyzed separately. PCB52-treated larvae had increased SLC bend
394 angles ($p > .0001$) at two intermediate stimulus intensities (38 and 41 dB) while PCB126 larvae
395 had increased SLC bend angles at the three highest stimulus intensities (**Figure S7**).
396 Furthermore, PCB153 (1000 nM) exposure resulted in an increased SLC bend angle at the
397 highest stimulus intensity for those few larvae that exhibited an SLC (n = 26 of 138, 43 dB, $p <$
398 $.0456$). LLC bend angle was significantly decreased across all stimulus intensities for PCB118.
399 It is not clear how bend angle is associated with altered signaling and cellular function.

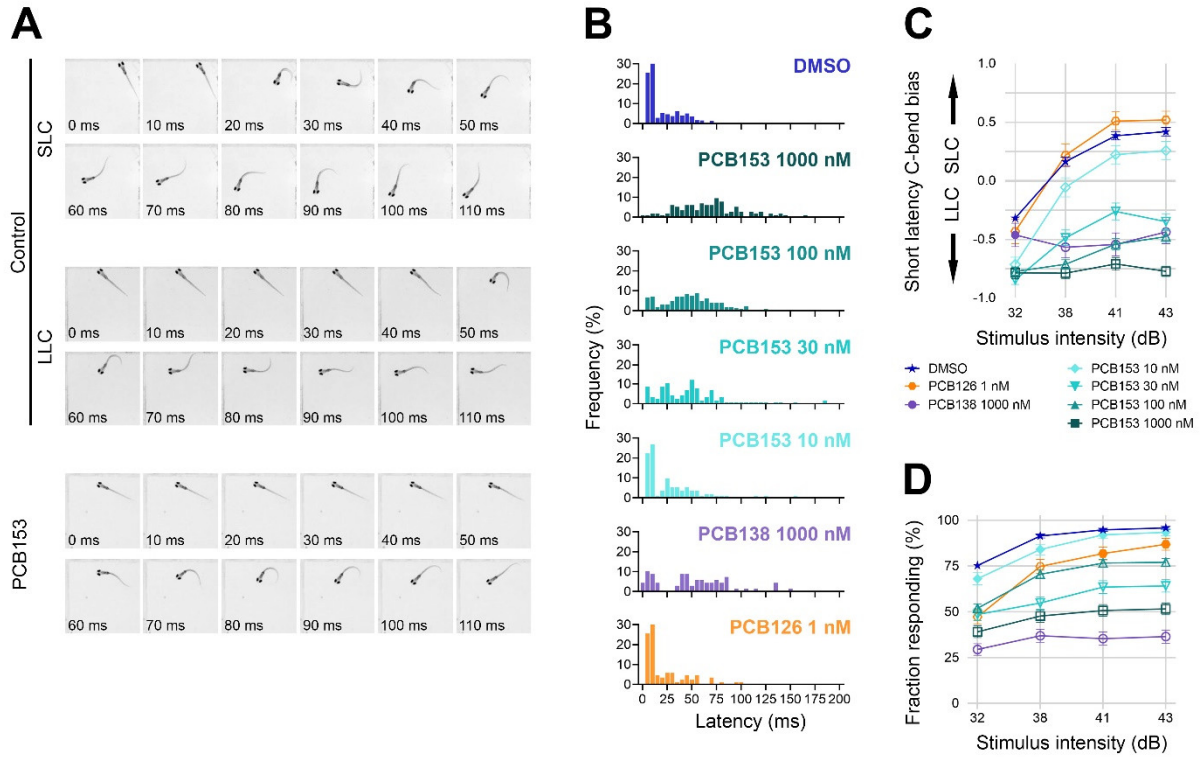

400 **Figure 2. Effect of PCBs on startle response in 6 dpf zebrafish.** (**A**) Representative short-
401 latency C-bend (SLC) and long-latency C-bend (LLC) startle response of a control zebrafish larva
402 at 6 dpf in comparison to a typical response of a PCB153 treated larva. (**B**) Vibro-acoustic startle
403 latency at highest stimulus intensity (43 dB) in vehigle control (*n* = 479), NDL-PCB153 1000 nM
404 (*n* = 179), NDL-PCB153 100 nM (*n* = 253), NDL-PCB153 30 nM (*n* = 152), NDL-PCB153 10 nM
405 (*n* = 119), NDL-PCB138 (*n* = 139), and DL-PCB126 (*n* = 97) exposed larvae. (**C**) Bias of SLC and
406 LLC and (**D**) response rate of different exposure groups at different vibro-acoustic intensities.
407 Values are presented as mean ± SEM. All data points are biologically independent replicates from
408 at least three independent experiments. Significant differences to DMSO controls ($p < 0.01$) are
409 indicated by open symbols.

410 ## 3.2 Cellular structures

411 The proper execution of the startle response relies on hair cells that sense the auditory stimulus,
412 M-cells to integrate the signals, and motor neurons and musculature to execute the startle
413 behavior. Morphological analysis showed that M-cells, motor neurons, and musculature all
414 appeared unaffected by PCB153, but the hair cell innervating neurons appeared to be swollen
415 (**Figure 3**). The L3 neuromast volume of control larvae was on average 569 μm^3 (*SD* = 125),
416 whereas PCB153-exposed larvae (1000 nM) had significantly larger L3 neuromast volumes 848
417 μm^3 (*SD* = 185), $t(48.93) = 6.765$, $p < .0001$ (**Figure 3B**). However, the number of hair cells in
418 L3 neuromasts (**Figure 3C**) and the intensity of FM1-43 dye internalized by hair cells (**Figure**
419 **3D**) remained unchanged in PCB153-treated larvae in comparison to the control.

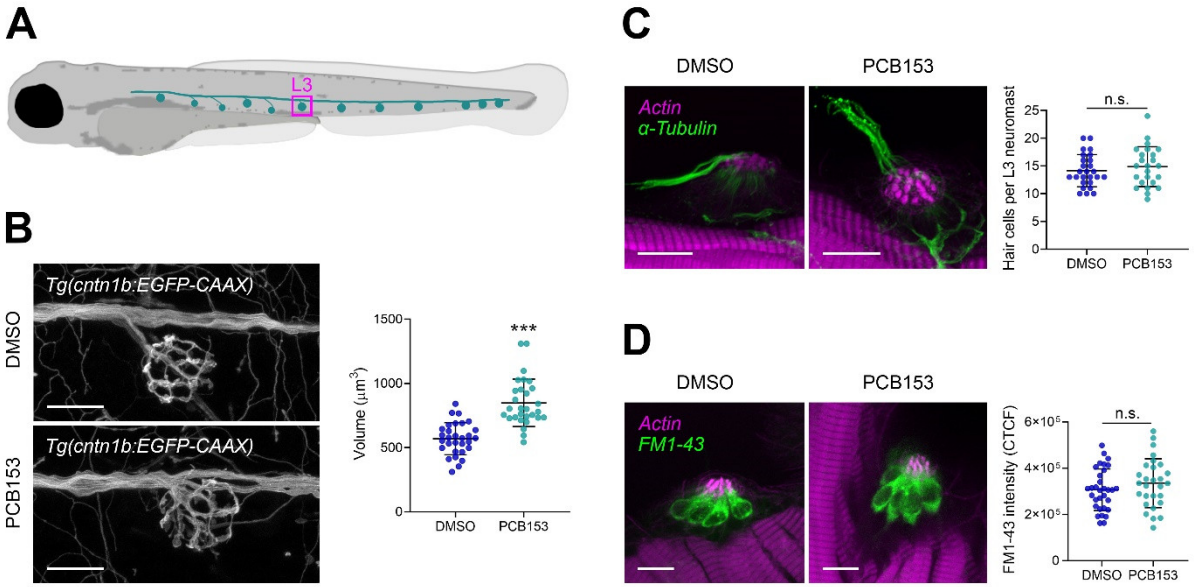

Figure 3. Effect of PCB153 on morphology and function of lateral line hair cells and innervating neurons. (**A**) Diagram indicating L3 neuromast. (**B**) Hair cell innervating neurons at neuromast L3 shown using *Tg(cntn1b:EGFP-CAAX)*. Volume of hair cell innervating neurons of DMSO (*n* = 30) and PCB153 (*n* = 29) treated larvae. Scale bar = 20 µm. (**C**) Whole-mount immune staining of kinocilia and hair cell innervating neurons (anti-acetylated tubulin antibody; green) and counterstain of stereocilia bundles and muscle tissue (actin; magenta) of DMSO (*n* = 26) and PCB153 (*n* = 24) treated larvae. The hair cell number was determined based on the number of kinocilia. Scale bar = 10 µm (**D**) Uptake of FM-143 dye as indication of functional hair cells of DMSO (*n* = 32) and PCB153 (*n* = 28) treated larvae. Scale bar = 10 µm. All data points are biologically independent replicates from at three independent experiments. Asterisks indicate significant differences to controls (***p < 0.0001).

The presence of M-cells is necessary for the SLC startle response. Staining with anti-3A10 confirmed the presence of M-cells in all PCB153-exposed larvae (21/21) (**Figure 4A**). We tested the functional responsiveness of the M-cells by applying electric field pulses to head-restrained larvae. This electrical stimulation bypasses the sensory system and directly activates the M-cell (Tabor et al., 2014). There was no difference detected in response time between control and 1000 nM PCB153-exposed larvae (U = 907.5, p = .489), demonstrating that the signal transmission from the M-cell to the motor neurons is not disrupted in PCR153-exposed fish

438 (**Figure S8A**). The fraction responding also was similar in both the DMSO-treated (290/299) and
439 the PCB153-treated (209/219) groups (GLM, p = .427; **Figure 4C, Figure S8B**). However, the
440 C-bend evoked by the electrical stimulation was larger in PCB153-exposed larvae (M = 101.4,
441 SD = 38.60) than in the control larvae (M = 83.12, SD = 24.23). An unpaired t-test with Welch-s
442 correction indicated that this difference was statistically significant, $t(74.27) = 2.679$, p =.0091
443 (**Figure S8C**). This difference could indicate a PCB153-evoked functional alteration of the M-cell
444 axon or motor neuron.

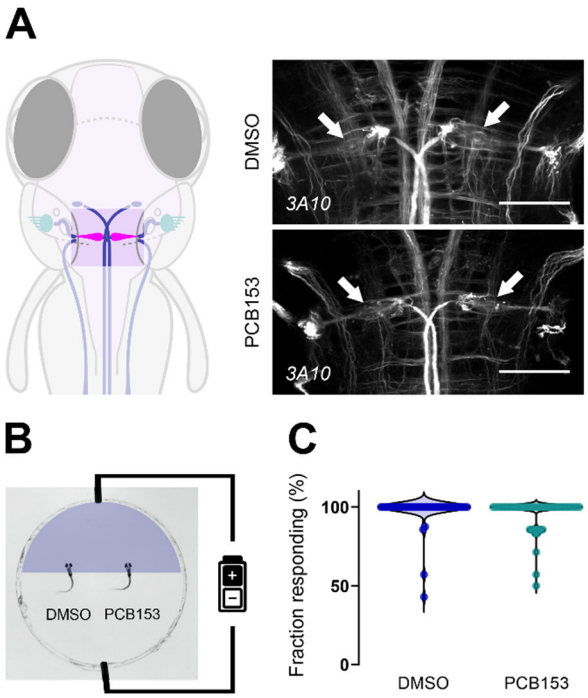

445 **Figure 4. Effect of PCB153 on morphology and function of the Mauthner-cells.** (**A**) Diagram
446 indicating localization of Mauthner-cells in the hindbrain. Brain tissue immunostaining with anti-
447 neurofilament 3A10 antibody labeling reticulospinal neurons in control and PCB153 treated larvae
448 at 6 dpf (ventral view). Mauthner (arrow) cells were present in all brain tissues (control: n = 23,
449 PCB153: n = 21). Scale bar = 50 µm. (**B**) Diagram of electrical stimulation performed to assess
450 the functionality of Mauthner-cells. (**C**) Percentage of responders to electrical stimulation. All data
451 points are biologically independent replicates from at least three independent experiments.

452 For rapid and effective axonal signal transmission, proper myelination of axons is key. We did
453 not find PCB153 to reduce cells of the oligodendrocyte lineage in the spinal cord, ($t(36) = .553$,
454 $p < .584$) nor any obvious differences in myelination itself (**Figure S9**).

455 Proper function and activation of the motor neurons is crucial for completion of the startle circuit,
456 leading to muscle contractions and the characteristic swimming behaviors. The main caudal
457 primary (CaP), middle primary (MiP), and rostral primary (RoP) motor neurons did not show any
458 distinct structural differences between exposed and control larvae (**Figure S10**). The fast
459 muscle fibers in the myotome were not found to be differentially striated in either treatment
460 groups (**Figure S11**). No structural difference in the motor neurons or the myotome was
461 apparent in PCB153-exposed larvae, suggesting that the increased bend angle does not
462 originate from any overt structural differences in the motor neurons or muscle fibers.

463 **3.3 Altered neural activity**

464 The release of neurotransmitters into the synaptic cleft is a characteristic process in signal
465 transmission. Both serotonergic and dopaminergic neuromodulators can affect startle latency
466 (Jain et al., 2018), and evidence has been found that NDL-PCBs alter these neuromodulators in
467 mammals (e.g. Castoldi et al. 2006; Enayah et al. 2018; Wigestrand et al. 2013). We observed
468 that PCB153 (1000 nM) altered the levels of several neurotransmitters in 6 dpf zebrafish larvae
469 (**Figure 5A**). Significantly increased level of GABA ($t(6) = 9.719$, $p < .001$), choline-chloride ($t(6)$
470 $= 8.459$, $p < .001$), 3-methoxytyramine hydrochloride ($t(6) = 3.803$, $p = .009$), and L-valine ($t(6) =$
471 3.134, $p = .020$) were measured in PCB-exposed larvae in comparison to control larvae; while
472 L-Glutamine was decreased in comparison to control larvae ($t(6) = 5.966$, $p < .001$).

473 To assess the interaction between PCB-exposure and changes in neuromodulatory activity, we
474 pharmacologically manipulated the neurotransmitter levels using dopamine, serotonin, and
475 GABA receptor agonists and antagonists. In control larvae, a 30 min exposure to dopamine

476 precursor L-DOPA and D2-receptor agonist Quinpirole, as well as serotonin precursor 5-HTP,
477 shifted the response to LLC, at multiple intensities tested ($p < .01$; **Figure 5C**). In contrast, the
478 dopamine antagonist haloperidol exposure induced a shift to SLC in controls across all stimulus
479 intensities ($p < .01$; **Figure 5C**). Haloperidol induced the same shift to SLC in PCB153-exposed
480 larvae ($p < .001$), suggesting that the startle circuit is functional but repressed by PCB (**Figure**
481 **5C**). The response rate remained unchanged after exposure to neurotransmitter modulators
482 except 5-HT, which caused an increase in response probability across all stimulus intensities in
483 control larvae ($p < .01$); Quinpirole, which caused a decrease in response probability at the two
484 lowest stimulus intensities in control larvae ($p < .01$); and Haloperidol, which caused an increase
485 in response probability at 41 dB in PCB153-treated larvae ($p < .01$; **Figure S6**). It is noteworthy,
486 that co-exposure to L-DOPA and PCB153 throughout development increased the response rate
487 of PCB153-treated larvae significantly ($p < .01$), yet only induced a significant shift towards SLC
488 at 38 dB ($p < .01$; **Figure S5C and S6C**).

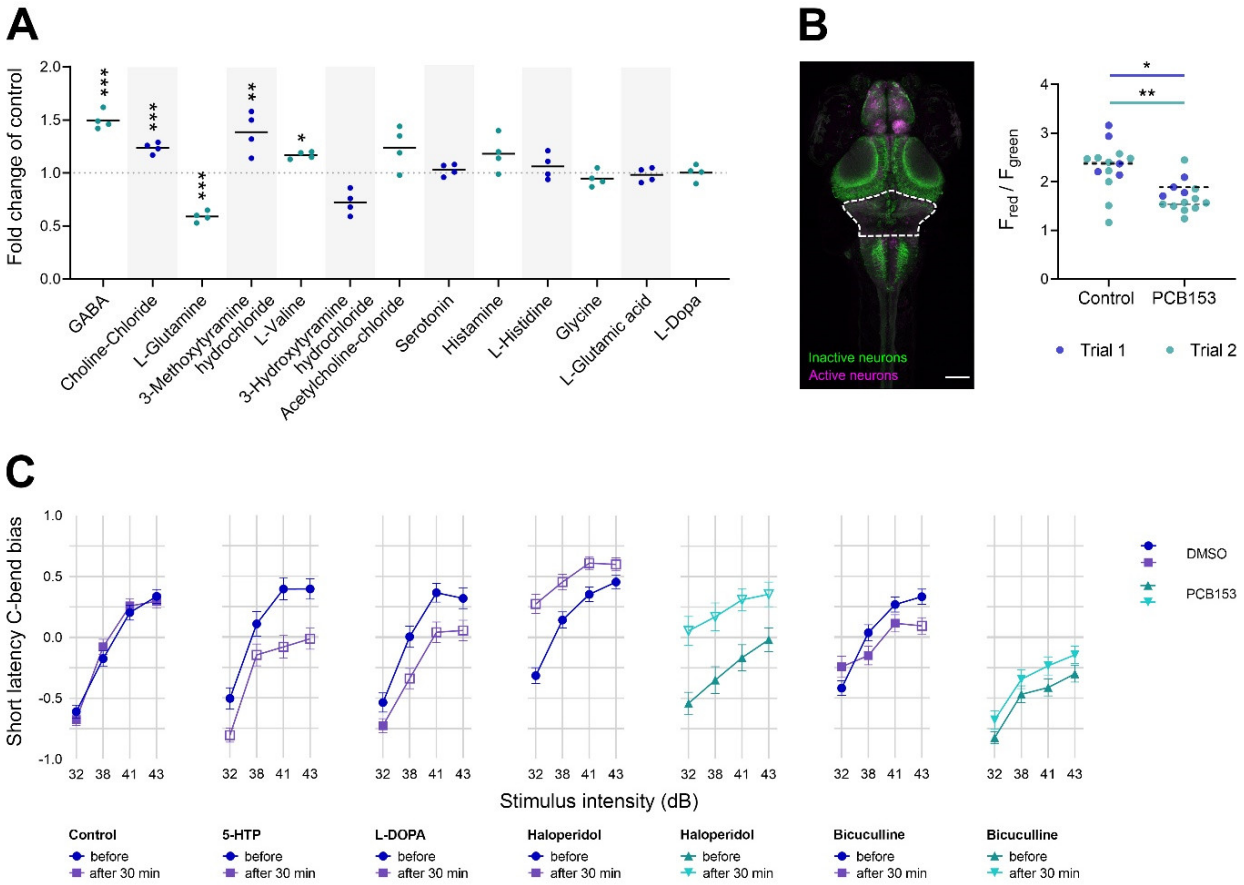

Figure 5. Involvement of neurotransmitters in startle latency. (**A**) Neurotransmitter levels in 6 dpf larvae exposed to 1000 nM PCB153 in comparison to control (*n* = 4). (**B**) Representative maximum intensity z-projection from confocal stack after photoconversions of freely swimming 6 dpf CaMPARI larvae. Scale bar = 100 µm. Ratio of red to green fluorescence intensity in the rostral hindbrain (indicated by dashed line in image) in DMSO (*n* = 14) and 1000 nM PCB153 (*n* = 14) exposed startling larvae in 4 ˚C (cold) medium. Dashed lines indicate median per trial. Two independent experiments. Asterisks indicate significant differences to controls (*p < 0.05, **p < 0.01, and ***p < 0.001). (**C**) Startle bias shift induced by 30-minute exposure to serotonin, dopamine, and GABA neurotransmitter modulators in 6 dpf control and 100 nM PCB153 exposed larvae. Control (*n* = 138-172), 5-HTP (*n* = 67-80), L-DOPA (*n* = 76-94), Haloperidol (Control *n* = 123-162, PCB153 *n* = 37-61), and Bicuculline (Control *n* = 90-162, PCB153 *n* = 83-137). All data points are biologically independent replicates from at least three independent experiments. Significant differences to respective controls (*p* < 0.01) are indicated by open symbols.

502 In the fish brain, a distinct population of serotonergic neurons is found in the posterior
503 tuberculum/hypothalamus, forming a prominent horseshoe-like pattern that is one of several
504 brain regions where 5-HT is synthesized (Oikonomou et al., 2019). To assess whether the
505 development of serotonergic cells in the brain of PCB153 larvae was affected, we performed
506 immunohistochemistry using an antibody for 5-HT (**Figure S12**). The intensity of the fluorescent
507 signal in the hypothalamus was not different, comparing PCB153 (M = 4.70 x 10^6, SD = 2.10 x
508 10^6) with the control (M = 4.38 x 10^6, SD = 8.1 x 10^5) group. This suggests that the serotonergic
509 neurons in this region were not affected.

510 During specific behaviors or sensory experiences, only a small percentage of neurons are
511 active. We analyzed the active neuronal cell populations in PCB153-treated and -untreated
512 larvae, focusing on the rostral hindbrain, where the M-cells are located, to assess whether there
513 were changes in neural activity. We examined neuronal activity using the CaMPARI zebrafish
514 line, which contains a protein that upon UV illumination permanently photoconverts from green
515 to red fluorescence in cells with high calcium levels (Fosque et al., 2015). This genomic tool
516 enabled us to look for active neuronal cell populations in larvae during normal swimming
517 movement, and in larvae experiencing a vibroacoustic stimulated startle response, both in
518 embryo medium at room temperature (24 °C), and at a colder temperature (4 °C). A higher red
519 to green ratio (F_{red}/F_{green}) was measured comparing cold medium with room temperature
520 medium: swimming control larvae in cold medium had a higher F_{red}/F_{green} ratio (M = 2.30, SD =
521 0.51) in comparison to swimming control larvae at RT (M = 0.96, SD = 0.17), confirming the
522 potential of cold medium to elicit higher neuronal activity (**Figure S13**). However, this difference
523 was diminished in PCB153-treated, yet still significant in trial 1: $F(1, 18) = 121$, *adj.* $p < .001$ and
524 trial 2: $F(1, 32) = 65.2$, *adj.* $p = .041$. Importantly, the difference between swimming control and
525 PCB153-treated larvae in cold medium was significant in both trial 1: $F(1, 18) = 121$, *adj.* p =
526 .028 and trial 2 $F(1, 32) = 65.2$, *adj.* $p < .001$ (**Figure 5**). Similar differences in neuronal activity

527 between control and PCB-153 treated larvae were measured for startling larvae during
528 photoconversion (**Figure S13**).

529 ## 4 Discussion

530 Despite most use ending decades ago, PCBs remain an important and persistent pollutant
531 impacting both wildlife and humans. To date, mechanistic studies of neurodevelopmental effects
532 of NDL-PCBs suggest two major targets: (1) alterations in neurotransmission, particularly
533 involving dopamine and serotonin, and consequently disruptions to Ca^{2+} signal transduction
534 (Campagna et al., 2011; Dervola et al., 2015; Enayah et al., 2018; Fonnum and Mariussen,
535 2009; Langeveld et al., 2012), and (2) loss of outer hair cells (Crofton et al., 2000; Trnovec et
536 al., 2010) or cochlear development (Goldey et al., 1995). However, such studies have not
537 addressed how PCBs exert developmental neurobehavioral deficits, and thus we do not know
538 whether neurobehavioral disorders resulting from prenatal exposure originate in a structural
539 effect in the auditory system, a neurotransmitter imbalance, or both. Furthermore, PCBs are
540 prevalent in aquatic ecosystems, yet we do not know the behavioral effects in fish and the
541 specificity of NDL-PCB congeners for these effects. In this study we used the zebrafish startle
542 response to comprehensively investigate the effects of different PCBs on neuron development
543 and signal transmission and to assess effects at environmentally relevant concentrations for
544 both humans and aquatic life.

545 The morphology of the neuronal cell body (perikaryal) and neurite provides essential information
546 on the developmental and physiological abnormalities in the neural circuits. We found that in
547 PCB153-exposed larvae, the neurons that innervate the hair cells had an increased volume
548 (**Figure 3**), indicating that PCB153 alters neuronal structure and hair cell function. Swelling of
549 afferent terminals is associated with hearing deficits in both mammalian models (Puel et al.,
550 1991) and zebrafish (Sebe et al., 2017). The increased volume may originate from increased

551 numbers of bulged (swollen) afferent neurite termini or increased arborization (branching). For
552 example, *tmie* mutant zebrafish, which are deaf with defective hair-cell function (Gleason et al.,
553 2009), have more complex peripheral arbors in afferent axons and an increased number of
554 neurites. In wildtype zebrafish, neurites with swollen axonal terminals are associated with hair
555 cells of both polarities rather than just a single polarity, suggesting a dysregulation of selection
556 in synaptic targets (Faucherre et al., 2010). At the sub-cellular level, neuronal swelling is due to
557 increased cationic permeability in neurons, causing an osmotic imbalance that leads to water
558 entry and cytotoxic edema (Rungta et al., 2015). While we examined a number of morphological
559 features of the startle circuit anatomy (hair cell, afferent neurons, M-cell, oligodendrocyte
560 lineage cells, myelination, motor neuron, muscle), only the volume of the neurons that innervate
561 the hair cells showed a measurable deviation in PCB153-exposed larvae. We thus infer that the
562 enlargement of axon termini is contributing to the neurotoxic potential of NDL-PCBs – an
563 understudied target of PCB toxicity. A few studies associate NDL-PCB exposure with altered
564 dendritic arborization (Lein et al., 2007; Yang et al., 2009). Axonal swelling is a pathology
565 appearing in many neurodegenerative disease (Coleman, 2005), and exposure to NDL-PCBs
566 may be a contributing factor in such diseases.

567 The startle response in fish and amphibians is a fundamental mechanism involved in predator
568 escape. Acoustic stimuli can trigger two distinct motor behaviors: a short-latency C-bend (SLC**;**
569 **Figure 2A**) initiated within 5-15 ms of the stimulus, or a long-latency C-bend (LLC; **Figure 2A**),
570 initiated within 15-100 ms (Burgess and Granato, 2007). At the structural level, laser-ablation of
571 the M-cell abolishes SLC responses without affecting LLC responses (Lacoste et al., 2015),
572 suggesting that the LLC is a 'backup' response (Burgess and Granato, 2007). The finding that
573 NDL-PCB-exposed larvae predominantly exhibit LLC without loss of M-cells (**Figure 4A**),
574 suggests that the M-cells are receiving a delayed input, are not firing properly, or that the signal
575 propagation downstream of the M-cell is disrupted. To distinguish these, we directly activated

576 the M-cells by applying electrical stimulation to control larvae with their heads restrained, and
577 found that unlike auditory stimulation, PCB153-exposed fish had latencies indistinguishable
578 from the controls. Furthermore, direct stimulation of PCB153-exposed larvae resulted in a
579 normal response rate and response time, although the bend angle was significantly increased.
580 These results indicate a proper function of M-cells in NDL-PCB-treated larvae. However, the
581 changes in bend angles we observed during these responses could indicate alterations
582 downstream of the M-cells.

583 There is less known about the mechanisms leading to an aberrant turning angle. Since we
584 found no obvious structural impairment downstream of the M-cell (oligodendrocyte lineage cells,
585 myelination, motor neuron, musculature), we speculate that the increased bend angle in
586 electrically stimulated larvae exposed to PCB153 may be linked to a sub-cellular disruption such
587 as gap junctions. It is known that PCBs can alter gap junction function in cells of many organs
588 (Bager et al., 1997; Kang et al., 1996; Machala et al., 2003) including NDL-PCB specific
589 inhibition of gap junctional intercellular communication in neural crest cells (Nyffeler et al., 2018)
590 and neuronal stem cells (PCB153; (Kang et al., 2001)). Gap junctions are intercellular channels
591 formed by connexins (Cx). RNA sequencing of zebrafish larvae exposed to PCB153 in a similar
592 exposure regime (4-120 hpf) and concentration (10 μM) significantly altered the expression of
593 connexin genes cx28.9, cx42, and cx35b (Aluru et al., 2020). Cx35 is expressed on the
594 Mauthner neuron lateral dendrites in zebrafish (Jain et al., 2018) and plays a crucial role in
595 regulating spinal motor activity during fast motor behavior of adult mosquitofish (Serrano-Velez
596 et al., 2014). We thus propose that gap junction function could be disrupted, which may be a
597 future study direction using single-cell RNA sequencing or genetically encoded optogenetics
598 that has yet to be developed in a model organism (Dong et al., 2018).

599 Neurotransmitters also play a key role in the startle response. A previous screening of more
600 than 1000 pharmacologically active compounds identified serotonergic and dopaminergic

601 modulators among the largest class of drugs that shift bias between SLC and LLC startle
602 behavior (Jain et al., 2018). Specifically, acute exposure to the D3R agonist (7OHD) shifted the
603 startle bias from LLC to SLC, while exposure to a D3R antagonist (or a 5-HT1AR agonist)
604 shifted bias toward LLC behavior (Jain et al., 2018). Our results extend these findings, showing
605 that 30 minutes exposure to L-DOPA or 5-HTP induces a shift from SLC to LLC at higher
606 stimulus intensities, as opposed to the D2R antagonist haloperidol, which evoked a shift to a
607 stronger SLC bias at all stimulus intensities (**Figure 5C**). NDL-PCBs are thought to affect
608 dopaminergic pathways (Mariussen and Fonnum, 2001; Tanaka et al., 2018; Wigestrand et al.,
609 2013), which is partly supported by our measurements of catecholamines and traces amines.
610 Specifically, we found that the extracellular dopamine metabolite 3-methoxytyramine
611 hydrochloride and the inhibitory transmitter GABA were significantly increased (**Figure 5A**). The
612 interplay between dopamine and GABA receptors activity is complex. In the mammalian system,
613 dopamine is a direct-acting modulator of $GABA_A$Rs (Hoerbelt et al., 2015). The simultaneous
614 presence of a dopamine metabolite and GABA in PCB153-exposed zebrafish larvae may
615 indicate that increased levels of GABA are a downstream effect of dysregulated dopamine
616 activity. With both dopamine and GABA playing critical roles in motor activity, we hypothesize
617 that PCB153 impairs dopaminergic neurotransmission and subsequently increases GABA
618 levels, leading to the predominant LLC response. One of the most crucial regulators of synapse
619 development and function mediating the GABAergic, dopaminergic, and serotonergic synaptic
620 transmission is the brain derived neurotrophic factor (BDNF). PCB153 induced the expression
621 of *bdnf* in zebrafish larvae (Aluru et al. 2020) suggesting BDNF as potential target for
622 transcriptional regulation. Furthermore, we propose that GABA is involved in the swelling of the
623 afferent terminals (**Figure 3**) as GABA activates Cl^- channels leading to an influx of Cl^-
624 accompanied by H_2O (Cesetti et al., 2012; Rungta et al., 2015). The osmotic neuronal swelling
625 alters neuronal activity. This study thus provides new evidence that GABA is involved in the

626 neurobehavioral mode of action of higher chlorinated NDL-PCBs, as has been for lower
627 chlorinated congeners (Fernandes et al., 2010).

628 An important finding of this study is that PCB153-exposed larvae can execute SLC when treated
629 with haloperidol, a D2-antagonist that can increase dopamine turnover in acute exposure
630 (Magnusson et al., 1987). There is a large body of evidence showing that NDL-PCBs, including
631 PCB153, modulate dopaminergic neurotransmission by inhibiting the dopamine precursor
632 enzyme tyrosine hydroxylase and dopamine synthesis itself, in both neural crest cells and adult
633 laboratory animal models including non-human primates (Dervola et al., 2015; Enayah et al.,
634 2018; Fonnum and Mariussen, 2009; Seegal et al., 1990). In zebrafish larvae, PCB153
635 exposure during development elicited differential expression of nine genes related to the
636 dopamine pathway, including tyrosine hydroxylase 2 (th2) (Aluru et al., 2020). Yet linking such
637 effects to behavior is rare. Tanaka et al. (2018) suggested that the NDL-PCB dominant mixture
638 Aroclor 1254 and BDE-47 functionally inhibited dopaminergic neurons in early zebrafish
639 embryos, as increased activity in 26 hpf embryos was inhibited by supplementation with L-
640 tyrosine and L-DOPA (Tanaka et al., 2018).

641 The restoration of the delayed startle phenotype by haloperidol, together with the increased
642 levels of a dopamine metabolite and GABA in PCB153-exposed larvae (**Figure 5A**), indicates
643 that disruption of dopaminergic and GABAergic signaling between neurons of the auditory circuit
644 is the dominant effect of PCB153-mediated aberrant motor behavior. These signaling processes
645 are widely conserved across vertebrate species, and are important in human neurological
646 diseases. For example, a recent study found that multiple gene mutations causing defective
647 startle response in zebrafish were also associated with disorders of the locomotor system in
648 humans (Meserve et al., 2020).

649 The localization of the PCB-induced disruption of dopaminergic signal transmission is likely
650 downstream of the hair cells, potentially in the hindbrain. Although dopaminergic neurons
651 innervate lateral line neuromasts, where D1R antagonist reduces the hair cell activity (Toro et
652 al., 2015), we found no difference in the hair cell activity of PCB153-exposed larvae (**Figure**
653 **3D**). This is in contrast to the hindbrain, where neuronal activity was reduced in PCB153
654 exposed CaMPARI zebrafish larvae (**Figure 5**), indicating a reduced capacity for release or
655 turnover of calcium. Intracellular Ca^{2+} signaling in neurons controls neurotransmitter secretion
656 among many other cellular processes and thus may be indirectly involved in dopamine or GABA
657 regulation. Some NDL-PCBs (PCB 95, 138) are known to inhibit voltage-gated calcium channels
658 (Langeveld et al., 2012) contributing to interference with calcium homeostasis and consequently
659 neurotransmission and synaptic plasticity (Brunelli et al., 2012; Campagna et al., 2011; Gafni et
660 al., 2003; Ta et al., 2006).

661 The startle response to threatening stimuli is vital for survival. PCB153-exposed zebrafish larvae
662 predominantly responded with a LLC, which not only delays the response, increasing the
663 chance to be caught by a predator, but also usually does not displace the animal from its
664 original location (**Figure 2A** and Jain et al., 2018). While survival of predator attack is likely
665 context-dependent and species-specific, escaping fast and away from a predator increases
666 survival in the field (McCormick et al., 2018). This suggests that exposure to NDL-PCBs may
667 alter selection pressure and thereby shift population structure. We have observed a significantly
668 delayed startle response at concentrations as low as 10 nM (3.6 µg L^{-1}). PCBs are associated
669 with sediments, where concentrations of PCB153 frequently reach multiple µg kg^{-1} (Lai et al.,
670 2015). PCB concentrations in organisms may be even higher due to extensive bioconcentration
671 (Killifish from New Bedford Harbor have 6.5 to 7 µg of PCB153 per g wet weight; Gräns et al.
672 2015). All NDL-PCBs tested in this study increased the startle latency. Thus, in the environment,
673 where PCBs occur in mixtures of numerous congeners that likely have additive effects, the

674 effect concentration is suggested to be lower than that of single congeners. Taken together,
675 these results highlight the importance of the neurotoxic potential of NDL-PCBs in an ecological
676 context.

677 In conclusion, the comprehensive approach presented here suggests that NDL-PCBs alter
678 dopamine signaling, leading to an increase in GABA that ultimately results in swelling of axonal
679 terminals in the auditory circuit. While the involvement of connexins remains speculative, our
680 findings provide a foothold into the dopamine dysregulating potential of NDL-PCBs in sensory-
681 motor processing in developing vertebrates, and link that to motor behavior. In a direct
682 comparison, the present study demonstrates that the adverse behavioral effects are induced by
683 all NDL-PCBs tested, but not by the classical DL-PCB126. Whether this is true for compounds
684 that are structurally similar to NDL-PCBs, such as some PBDEs, is not known and will require
685 further research. A key finding is that the effect of NDL-PCBs on the startle latency occurs at
686 concentrations relevant for both environmental and human exposures, and therefore may
687 contribute to the selection pressure in the environment and neurotoxicological disease in
688 human. This study provides valuable clues for tackling health effects in humans and wildlife
689 caused by environmental exposure.

690 **CRediT authorship contribution statement**

691 **Nadja R. Brun:** Conceptualization, Methodology, Formal analysis, Investigation, Writing - original
692 draft, Writing - review & editing, Visualization, Funding acquisition. **Jennifer M. Panlilio:**
693 Conceptualization, Methodology, Software, Formal analysis, Investigation, Writing - review &
694 editing, Funding acquisition. **Kun Zhang:** Methodology, Investigation, Writing - review & editing,
695 Funding acquisition. **Yanbin Zhao:** Methodology, Investigation, Writing - review & editing,
696 Funding acquisition. **Evgeny Ivashkin:** Methodology, Investigation. **John J. Stegeman:**

Conceptualization, Writing - review & editing, Funding acquisition. **Jared V. Goldstone:** Conceptualization, Writing - review & editing, Project administration.

Competing Financial Interests

The authors declare they have no actual or potential competing financial interests.

Funding

This work was supported by the Swiss National Science Foundation P2EZP2_165200 (NRB), the Boston University Superfund Research Program NIH 5P42ES007381 (JJS and JVG), the Woods Hole Center for Oceans and Human Health (NIH: P01ES021923 and P01ES028938; NSF: OCE-1314642 and OCE-1840381) (NRB, JMP and JJS), and the National Natural Science Foundation of China 22006099 (KZ and YZ) and the Shanghai Pujiang Program 19PJ1404900 (KZ and YZ).

Acknowledgments

The authors would like to thank Neel Aluru for helpful discussion and providing the confocal microscope and Ed Levin and Mark Hahn for critically reading the manuscript and making valuable suggestions.

References

Almeida, R.G., Czopka, T., Ffrench-Constant, C., Lyons, D.A., 2011. Individual axons regulate the myelinating potential of single oligodendrocytes in vivo. Development 138, 4443–50. https://doi.org/10.1242/dev.071001

Aluru, N., Krick, K.S., Mcdonald, A.M., Karchner, S.I., 2020. Developmental exposure to PCB153 (2,2′,4,4′,5,5′-hexachlorobiphenyl) alters circadian rhythms and the expression of clock and metabolic genes. Toxicol. Sci. 173, 41–52. https://doi.org/10.1093/toxsci/kfz217

Bager, Y., Lindebro, M.C., Martel, P., Chaumontet, C., Wärngård, L., 1997. Altered function, localization and phosphorylation of gap junctions in rat liver epithelial, IAR 20, cells after treatment with PCBs or TCDD. Environ. Toxicol. Pharmacol. 3, 257–266. https://doi.org/10.1016/S1382-6689(97)00021-5

722 Bates, D., Mächler, M., Bolker, B., Walker, S., 2015. Fitting Linear Mixed-Effects Models using
723 lme4. J. Stat. Softw. 67, 1–48. https://doi.org/10.18637/jss.v067.i01

724 Berger, D.F., Lombardo, J.P., Jeffers, P.M., Hunt, A.E., Bush, B., Casey, A., Quimby, F., 2001.
725 Hyperactivity and impulsiveness in rats fed diets supplemented with either Aroclor 1248 or
726 PCB-contaminated St. Lawrence river fish. Behav. Brain Res. 126, 1–11.
727 https://doi.org/10.1016/S0166-4328(01)00244-3

728 Bergonzi, R., Specchia, C., Dinolfo, M., Tomasi, C., De Palma, G., Frusca, T., Apostoli, P.,
729 2009. Distribution of persistent organochlorine pollutants in maternal and foetal tissues:
730 Data from an Italian polluted urban area. Chemosphere 76, 747–754.
731 https://doi.org/10.1016/j.chemosphere.2009.05.026

732 Boix, J., Cauli, O., Felipo, V., 2010. Developmental exposure to polychlorinated biphenyls 52,
733 138 or 180 affects differentially learning or motor coordination in adult rats. Mechanisms
734 involved. Neuroscience 167, 994–1003. https://doi.org/10.1016/j.neuroscience.2010.02.068

735 Boucher, O., Muckle, G., Bastien, C.H., 2009. Prenatal exposure to polychlorinated biphenyls: A
736 neuropsychologic analysis. Environ. Health Perspect. 117, 7–16.
737 https://doi.org/10.1289/ehp.11294

738 Brunelli, L., LLansola, M., Felipo, V., Campagna, R., Airoldi, L., De Paola, M., Fanelli, R.,
739 Mariani, A., Mazzoletti, M., Pastorelli, R., 2012. Insight into the neuroproteomics effects of
740 the food-contaminant non-dioxin like polychlorinated biphenyls. J. Proteomics 75, 2417–
741 2430. https://doi.org/10.1016/J.JPROT.2012.02.023

742 Burgess, H.A., Granato, M., 2007. Sensorimotor gating in larval zebrafish. J. Neurosci. 27,
743 4984–4994. https://doi.org/10.1523/JNEUROSCI.0615-07.2007

744 Campagna, R., Brunelli, L., Airoldi, L., Fanelli, R., Hakansson, H., Heimeier, R.A., De Boever,
745 P., Boix, J., Llansola, M., Felipo, V., Pastorelli, R., 2011. Cerebellum Proteomics
746 addressing the cognitive deficit of rats perinatally exposed to the food-relevant
747 polychlorinated biphenyl 138. Toxicol. Sci. 123, 170–179.
748 https://doi.org/10.1093/toxsci/kfr156

749 Castoldi, A.F., Blandini, F., Randine, G., Samuele, A., Manzo, L., Coccini, T., 2006. Brain
750 monoaminergic neurotransmission parameters in weanling rats after perinatal exposure to
751 methylmercury and 2,2′,4,4′,5,5′-hexachlorobiphenyl (PCB153). Brain Res. 1112, 91–98.
752 https://doi.org/10.1016/j.brainres.2006.07.022

753 Cesetti, T., Ciccolini, F., Li, Y., 2012. GABA not only a neurotransmitter: Osmotic regulation by
754 GABA AR signaling. Front. Cell. Neurosci. https://doi.org/10.3389/fncel.2012.00003

755 Chen, Y.-C.J., Guo, Y.-L., Hsu, C.-C., Rogan, W.J., 1992. Cognitive development of Yu-Cheng
756 ('Oil Disease') children prenatally exposed to heat-degraded PCBs. JAMA J. Am. Med.
757 Assoc. 268, 3213. https://doi.org/10.1001/jama.1992.03490220057028

758 Coccini, T., Roda, E., Castoldi, A.F., Poli, D., Goldoni, M., Vettori, M.V., Mutti, A., Manzo, L.,
759 2011. Developmental exposure to methylmercury and 2,2′,4,4′,5,5′-hexachlorobiphenyl
760 (PCB153) affects cerebral dopamine D1-like and D2-like receptors of weanling and

761 pubertal rats. Arch. Toxicol. 85, 1281–1294. https://doi.org/10.1007/s00204-011-0660-y

762 Coleman, M., 2005. Axon degeneration mechanisms: Commonality amid diversity. Nat. Rev.
763 Neurosci. https://doi.org/10.1038/nrn1788

764 Crofton, K.M., Ding, D.-L., Padich, R., Taylor, M., Henderson, D., 2000. Hearing loss following
765 exposure during development to polychlorinated biphenyls: A cochlear site of action. Hear.
766 Res. 144, 196–204. https://doi.org/10.1016/S0378-5955(00)00062-9

767 Dervola, K.S.N., Johansen, E.B., Walaas, S.I., Fonnum, F., 2015. Gender-dependent and
768 genotype-sensitive monoaminergic changes induced by polychlorinated biphenyl 153 in the
769 rat brain. Neurotoxicology 50, 38–45. https://doi.org/10.1016/J.NEURO.2015.07.004

770 Dong, A., Liu, S., Li, Y., 2018. Gap junctions in the nervous system: Probing functional
771 connections using new imaging approaches. Front. Cell. Neurosci. 12, 1–9.
772 https://doi.org/10.3389/fncel.2018.00320

773 Enayah, S.H., Vanle, B.C., Fuortes, L.J., Doorn, J.A., Ludewig, G., 2018. PCB95 and PCB153
774 change dopamine levels and turn-over in PC12 cells. Toxicology 394, 93–101.
775 https://doi.org/10.1016/j.tox.2017.12.003

776 Ennaceur, S., Gandoura, N., Driss, M.R., 2008. Distribution of polychlorinated biphenyls and
777 organochlorine pesticides in human breast milk from various locations in Tunisia: Levels of
778 contamination, influencing factors, and infant risk assessment. Environ. Res. 108, 86–93.
779 https://doi.org/10.1016/J.ENVRES.2008.05.005

780 Faucherre, A., Baudoin, J.P., Pujol-Martí, J., López-Schier, H., 2010. Multispectral four-
781 dimensional imaging reveals that evoked activity modulates peripheral arborization and the
782 selection of plane-polarized targets by sensory neurons. Development 137, 1635–1643.
783 https://doi.org/10.1242/dev.047316

784 Fernandes, E.C.A., Hendriks, H.S., Van Kleef, R.G.D.M., Van Den Berg, M., Westerink, R.H.S.,
785 2010. Potentiation of the human GABAA receptor as a novel mode of action of lower-
786 chlorinated non-dioxin-like PCBs. Environ. Sci. Technol. 44, 2864–2869.
787 https://doi.org/10.1021/es902321a

788 Fonnum, F., Mariussen, E., 2009. Mechanisms involved in the neurotoxic effects of
789 environmental toxicants such as polychlorinated biphenyls and brominated flame
790 retardants. J. Neurochem. 111, 1327–1347. https://doi.org/10.1111/j.1471-
791 4159.2009.06427.x

792 Fosque, B.F., Sun, Y., Dana, H., Yang, C., Ohyama, T., Tadross, M.R., Patel, R., Zlatic, M.,
793 Kim, D.S., Ahrens, M.B., Jayaraman, V., Looger, L.L., Schreiter, E.R., 2015. Labeling of
794 active neural circuits in vivo with designed calcium integrators. Science (80-.). 347, 755–
795 760.

796 Gafni, J., Wong, P.W., Pessah, I.N., 2003. Non-coplanar 2,2',3,5',6-pentachlorobiphenyl (PCB
797 95) amplifies ionotropic glutamate receptor signaling in embryonic cerebellar granule
798 neurons by a mechanism involving ryanodine receptors. Toxicol. Sci. 77, 72–82.
799 https://doi.org/10.1093/toxsci/kfh004

800 Gleason, M.R., Nagiel, A., Jamet, S., Vologodskaia, M., López-Schier, H., Hudspeth, A.J., 2009.
801 The transmembrane inner ear (Tmie) protein is essential for normal hearing and balance in
802 the zebrafish. Proc. Natl. Acad. Sci. U. S. A. 106, 21347–21352.
803 https://doi.org/10.1073/pnas.0911632106

804 Goldey, E.S., Kehn, L.S., Lau, C., Rehnberg, G.L., Crofton, K.M., 1995. Developmental
805 exposure to polychlorinated biphenyls (Aroclor 1254) reduces circulating thyroid hormone
806 concentrations and causes hearing deficits in rats. Toxicol. Appl. Pharmacol. 135, 77–88.
807 https://doi.org/10.1006/TAAP.1995.1210

808 Grandjean, P., Landrigan, P.J., 2014. Neurobehavioural effects of developmental toxicity.
809 Lancet Neurol. 13, 330–338. https://doi.org/10.1016/S1474-4422(13)70278-3

810 Gräns, J., Wassmur, B., Fernández-Santoscoy, M., Zanette, J., Woodin, B.R., Karchner, S.I.,
811 Nacci, D.E., Champlin, D., Jayaraman, S., Hahn, M.E., Stegeman, J.J., Celander, M.C.,
812 2015. Regulation of pregnane-X-receptor, CYP3A and P-glycoprotein genes in the PCB-
813 resistant killifish (Fundulus heteroclitus) population from New Bedford Harbor. Aquat.
814 Toxicol. 159, 198–207. https://doi.org/10.1016/j.aquatox.2014.12.010

815 Herbstman, J.B., Sjödin, A., Apelberg, B.J., Witter, F.R., Patterson, D.G., Halden, R.U., Jones,
816 R.S., Park, A., Zhang, Y., Heidler, J., Needham, L.L., Goldman, L.R., 2007. Determinants
817 of prenatal exposure to polychlorinated biphenyls (PCBs) and polybrominated diphenyl
818 ethers (PBDEs) in an urban population. Environ. Health Perspect. 115, 1794–1800.
819 https://doi.org/10.1289/ehp.10333

820 Hoerbelt, P., Lindsley, T.A., Fleck, M.W., 2015. Dopamine directly modulates GABAA receptors.
821 J. Neurosci. 35, 3525–3536. https://doi.org/10.1523/JNEUROSCI.4390-14.2015

822 Howe, K., Clark, M.D., Torroja, C.F., Torrance, J., Berthelot, C., Muffato, M., Collins, J.E.,
823 Humphray, S., McLaren, K., Matthews, L., McLaren, S., Sealy, I., Caccamo, M., Churcher,
824 C., Scott, C., Barrett, J.C., Koch, R., Rauch, G.-J., White, S., Chow, W., Kilian, B., Quintais,
825 L.T., Guerra-Assunção, J. a, Zhou, Y., Gu, Y., Yen, J., Vogel, J.-H., Eyre, T., Redmond, S.,
826 Banerjee, R., Chi, J., Fu, B., Langley, E., Maguire, S.F., Laird, G.K., Lloyd, D., Kenyon, E.,
827 Donaldson, S., Sehra, H., Almeida-King, J., Loveland, J., Trevanion, S., Jones, M., Quail,
828 M., Willey, D., Hunt, A., Burton, J., Sims, S., McLay, K., Plumb, B., Davis, J., Clee, C.,
829 Oliver, K., Clark, R., Riddle, C., Elliot, D., Eliott, D., Threadgold, G., Harden, G., Ware, D.,
830 Begum, S., Mortimore, B., Mortimer, B., Kerry, G., Heath, P., Phillimore, B., Tracey, A.,
831 Corby, N., Dunn, M., Johnson, C., Wood, J., Clark, S., Pelan, S., Griffiths, G., Smith, M.,
832 Glithero, R., Howden, P., Barker, N., Lloyd, C., Stevens, C., Harley, J., Holt, K.,
833 Panagiotidis, G., Lovell, J., Beasley, H., Henderson, C., Gordon, D., Auger, K., Wright, D.,
834 Collins, J., Raisen, C., Dyer, L., Leung, K., Robertson, L., Ambridge, K., Leongamornlert,
835 D., McGuire, S., Gilderthorp, R., Griffiths, C., Manthravadi, D., Nichol, S., Barker, G.,
836 Whitehead, S., Kay, M., Brown, J., Murnane, C., Gray, E., Humphries, M., Sycamore, N.,
837 Barker, D., Saunders, D., Wallis, J., Babbage, A., Hammond, S., Mashreghi-Mohammadi,
838 M., Barr, L., Martin, S., Wray, P., Ellington, A., Matthews, N., Ellwood, M., Woodmansey,
839 R., Clark, G., Cooper, J.D., Cooper, J., Tromans, A., Grafham, D., Skuce, C., Pandian, R.,
840 Andrews, R., Harrison, E., Kimberley, A., Garnett, J., Fosker, N., Hall, R., Garner, P., Kelly,
841 D., Bird, C., Palmer, S., Gehring, I., Berger, A., Dooley, C.M., Ersan-Ürün, Z., Eser, C.,
842 Geiger, H., Geisler, M., Karotki, L., Kirn, A., Konantz, J., Konantz, M., Oberländer, M.,
843 Rudolph-Geiger, S., Teucke, M., Lanz, C., Raddatz, G., Osoegawa, K., Zhu, B., Rapp, A.,

Widaa, S., Langford, C., Yang, F., Schuster, S.C., Carter, N.P., Harrow, J., Ning, Z., Herrero, J., Searle, S.M.J., Enright, A., Geisler, R., Plasterk, R.H. a, Lee, C., Westerfield, M., de Jong, P.J., Zon, L.I., Postlethwait, J.H., Nüsslein-Volhard, C., Hubbard, T.J.P., Roest Crollius, H., Rogers, J., Stemple, D.L., 2013. The zebrafish reference genome sequence and its relationship to the human genome. Nature 496, 498–503. https://doi.org/10.1038/nature12111

Hudspeth, A., 1985. The cellular basis of hearing: the biophysics of hair cells. Science (80-.). 230, 745–752. https://doi.org/10.1126/science.7414321

Inoue, D., Wittbrodt, J., 2011. One for all-a highly efficient and versatile method for fluorescent immunostaining in fish embryos. PLoS One 6, 1–7. https://doi.org/10.1371/journal.pone.0019713

Jain, R.A., Wolman, M.A., Marsden, K.C., Nelson, J.C., Shoenhard, H., Echeverry, F.A., Szi, C., Bell, H., Skinner, J., Cobbs, E.N., Sawada, K., Zamora, A.D., Pereda, A.E., Granato, M., 2018. A forward genetic screen in zebrafish identifies the G-protein-coupled receptor CaSR as a modulator of sensorimotor decision making. Curr. Biol. 28, 1357-1369.e5. https://doi.org/10.1016/j.cub.2018.03.025

Johansen, E.B., Fonnum, F., Lausund, P.L., Walaas, S.I., Bærland, N.E., Wøien, G., Sagvolden, T., 2014. Behavioral changes following PCB 153 exposure in the Spontaneously Hypertensive rat - an animal model of Attention-Deficit/Hyperactivity disorder. Behav. Brain Funct. 10, 1–19. https://doi.org/10.1186/1744-9081-10-1

Jusko, T.A., Sisto, R., Iosif, A.-M., Moleti, A., Wimmerová, S., Lancz, K., Tihányi, J., Šovčiková, E., Drobná, B., Palkovičová, L., Jurečková, D., Thevenet-Morrison, K., Verner, M.-A., Sonneborn, D., Hertz-Picciotto, I., Trnovec, T., 2014. Prenatal and postnatal serum PCB concentrations and cochlear function in children at 45 months of age. Environ. Health Perspect. 122, 1246–1252. https://doi.org/10.1289/ehp.1307473

Kang, K.-S., Park, J.-E., Ryu, D.-Y., Lee, Y.-S., 2001. Effects and neuro-toxic mechanisms of 2,2',4,4',5,5'-hexachlorobiphenyl and endosulfan in neuronal stem cells. J. Vet. Med. Sci. 63, 1183–1190. https://doi.org/10.1292/jvms.63.1183

Kang, K.S., Wilson, M.R., Hayashi, T., Chang, C.C., Trosko, J.E., 1996. Inhibition of gap junctional intercellular communication in normal human breast epithelial cells after treatment with pesticides, PCBs, and PBBs, alone or in mixtures. Environ. Health Perspect. 104, 192–200. https://doi.org/10.1289/ehp.96104192

Kimmel, C.B., 1993. Patterning the brain of the zebrafish embryo. Annu. Rev. Neurosci. 16, 707–732. https://doi.org/10.1146/annurev.ne.16.030193.003423

Lacoste, A.M.B., Schoppik, D., Robson, D.N., Haesemeyer, M., Portugues, R., Li, J.M., Randlett, O., Wee, C.L., Engert, F., Schier, A.F., 2015. A convergent and essential interneuron pathway for mauthner-cell-mediated escapes. Curr. Biol. 25, 1526–1534. https://doi.org/10.1016/j.cub.2015.04.025

Lai, Z., Li, X., Li, H., Zhao, L., Zeng, Y., Wang, C., Gao, Y., Liu, Q., 2015. Residual distribution and risk assessment of polychlorinated biphenyls in surface sediments of the Pearl River

Delta, South China. Bull. Environ. Contam. Toxicol. 95, 37–44. https://doi.org/10.1007/s00128-015-1563-z

Lancz, K., Hertz-Picciotto, I., Jusko, T.A., Murínová, Ľ., Wimmerová, S., Šovčíková, E., Dedík, L., Strémy, M., Drobná, B., Farkašová, D., Trnovec, T., 2015a. Duration of breastfeeding and serum PCB 153 concentrations in children. Environ. Res. 136, 35–39. https://doi.org/10.1016/j.envres.2014.09.036

Lancz, K., Palkovičováa, L., Patayová, H., Drobná, B., Wimmerová, S., Šovčíková, E., Kováč, J., Farkašová, D., Hertz-Picciotto, I., Jusko, T.A., Trnovec, T., 2015b. Ratio of cord to maternal serum PCB concentrations in relation to their congener-specific physicochemical properties. Int J Hyg Env. Heal. 218, 91–98. https://doi.org/doi:10.1016/j.ijheh.2014.08.003

Landrigan, P.J., Fuller, R., Acosta, N.J.R., Adeyi, O., Arnold, R., Basu, N., Baldé, A.B., Bertollini, R., Bose-O'Reilly, S., Boufford, J.I., Breysse, P.N., Chiles, T., Mahidol, C., Coll-Seck, A.M., Cropper, M.L., Fobil, J., Fuster, V., Greenstone, M., Haines, A., Hanrahan, D., Hunter, D., Khare, M., Krupnick, A., Lanphear, B., Lohani, B., Martin, K., Mathiasen, K. V., McTeer, M.A., Murray, C.J.L., Ndahimananjara, J.D., Perera, F., Potočnik, J., Preker, A.S., Ramesh, J., Rockström, J., Salinas, C., Samson, L.D., Sandilya, K., Sly, P.D., Smith, K.R., Steiner, A., Stewart, R.B., Suk, W.A., van Schayck, O.C.P., Yadama, G.N., Yumkella, K., Zhong, M., 2018. The Lancet Commission on pollution and health. Lancet 391, 462–512. https://doi.org/10.1016/S0140-6736(17)32345-0

Langeveld, W.T., Meijer, M., Westerink, R.H.S., 2012. Differential effects of 20 non-dioxin-like PCBs on basal and depolarization-evoked intracellular calcium levels in PC12 cells. Toxicol. Sci. 126, 487–496. https://doi.org/10.1093/toxsci/kfr346

Lein, P.J., Yang, D., Bachstetter, A.D., Tilson, H.A., Harry, G.J., Mervis, R.F., Kodavanti, P.R.S., 2007. Ontogenetic alterations in molecular and structural correlates of dendritic growth after developmental exposure to polychlorinated biphenyls. Environ. Health Perspect. 115, 556–563. https://doi.org/10.1289/ehp.9773

Lilienthal, H., Heikkinen, P., Andersson, P.L., van der Ven, L.T.M., Viluksela, M., 2011. Auditory effects of developmental exposure to purity-controlled polychlorinated biphenyls (PCB52 and PCB180) in rats. Toxicol. Sci. 122, 100–111. https://doi.org/10.1093/toxsci/kfr077

Lilienthal, H., Korkalainen, M., Andersson, P.L., Viluksela, M., 2015. Developmental exposure to purity-controlled polychlorinated biphenyl congeners (PCB74 and PCB95) in rats: Effects on brainstem auditory evoked potentials and catalepsy. Toxicology 327, 22–31. https://doi.org/10.1016/J.TOX.2014.11.004

Liu, Y.C., Hale, M.E., 2017. Local spinal cord circuits and bilateral mauthner cell activity function together to drive alternative startle behaviors. Curr. Biol. 27, 697–704. https://doi.org/10.1016/j.cub.2017.01.019

Machala, M., Bláha, L., Vondráček, J., Trosko, J.E., Scott, J., Upham, B.L., 2003. Inhibition of gap junctional intercellular communication by noncoplanar polychlorinated biphenyls: Inhibitory potencies and screening for potential Mode(s) of Action. Toxicol. Sci. 76, 187–195. https://doi.org/10.1093/TOXSCI

924 Magnusson, O., Mohringe, B., Thorell, G., Lake-Bakaar, D.M., 1987. Effects of the dopamine D2
925 selective receptor antagonist remoxipride on dopamine turnover in the rat brain after acute
926 and repeated administration. Pharmacol. Toxicol. 60, 368–373.
927 https://doi.org/10.1111/j.1600-0773.1987.tb01529.x

928 Mariussen, E., Fonnum, F., 2001. The effect of polychlorinated biphenyls on the high affinity
929 uptake of the neurotransmitters, dopamine, serotonin, glutamate and GABA, into rat brain
930 synaptosomes. Toxicology 159, 11–21. https://doi.org/10.1016/S0300-483X(00)00374-7

931 Maximino, C., Herculano, A.M., 2010. A review of monoaminergic neuropsychopharmacology in
932 zebrafish. Zebrafish 7, 359–378. https://doi.org/10.1089/zeb.2010.0669

933 McCormick, M.I., Fakan, E., Allan, B.J.M., 2018. Behavioural measures determine survivorship
934 within the hierarchy of whole-organism phenotypic traits. Funct. Ecol. 32, 958–969.
935 https://doi.org/10.1111/1365-2435.13033

936 Medan, V., Preuss, T., 2014. The Mauthner-cell circuit of fish as a model system for startle
937 plasticity. J. Physiol. Paris 108, 129–140. https://doi.org/10.1016/j.jphysparis.2014.07.006

938 Meserve, J.H., Nelson, J.C., Marsden, K.C., Hsu, J., Echeverry, F.A., Jain, A., Wolman, M.A.,
939 Pereda, A.E., Granato, M., 2020. A forward genetic screen identifies Dolk as a regulator of
940 startle magnitude through the potassium channel subunit Kv1.1. bioRxiv.

941 Meyers, J.R., MacDonald, R.B., Duggan, A., Lenzi, D., Standaert, D.G., Corwin, J.T., Corey,
942 D.P., 2003. Lighting up the senses: FM1-43 loading of sensory cells through nonselective
943 ion channels. J. Neurosci. 23, 4054–65. https://doi.org/10.1523/JNEUROSCI.23-10-
944 04054.2003

945 Nakayama, H., 2004. Common sensory inputs and differential excitability of segmentally
946 homologous reticulospinal neurons in the hindbrain. J. Neurosci. 24, 3199–3209.
947 https://doi.org/10.1523/JNEUROSCI.4419-03.2004

948 Nyffeler, J., Chovancova, P., Dolde, X., Holzer, A.K., Purvanov, V., Kindinger, I., Kerins, A.,
949 Higton, D., Silvester, S., van Vugt-Lussenburg, B.M.A., Glaab, E., van der Burg, B.,
950 Maclennan, R., Legler, D.F., Leist, M., 2018. A structure–activity relationship linking non-
951 planar PCBs to functional deficits of neural crest cells: new roles for connexins. Arch.
952 Toxicol. 92, 1225–1247. https://doi.org/10.1007/s00204-017-2125-4

953 Oikonomou, G., Altermatt, M., Zhang, R. wei, Coughlin, G.M., Montz, C., Gradinaru, V., Prober,
954 D.A., 2019. The Serotonergic Raphe Promote Sleep in Zebrafish and Mice. Neuron 103,
955 686-701.e8. https://doi.org/10.1016/j.neuron.2019.05.038

956 Panlilio, J.M., Aluru, N., Hahn, M.E., 2020. Developmental Neurotoxicity of the Harmful Algal
957 Bloom Toxin Domoic Acid: Cellular and Molecular Mechanisms Underlying Altered
958 Behavior in the Zebrafish Model. Environ. Health Perspect. 128, 117002.
959 https://doi.org/10.1289/EHP6652

960 Panlilio, J.M., Jones, I.T., Salanga, M.C., Aluru, N., Hahn, M.E., 2021. Developmental exposure
961 to domoic acid disrupts startle response behavior and circuitry. bioRxiv.
962 https://doi.org/10.1101/2021.01.08.425996

963 Park, H.-C., Shin, J., Roberts, R.K., Appel, B., 2007. An olig2 reporter gene marks
964 oligodendrocyte precursors in the postembryonic spinal cord of zebrafish. Dev. Dyn. 236,
965 3402–3407. https://doi.org/10.1002/dvdy.21365

966 Poon, E., Bandara, S.B., Allen, J.B., Sadowski, R.N., Schantz, S.L., 2015. Developmental PCB
967 exposure increases susceptibility to audiogenic seizures in adulthood. Neurotoxicology 46,
968 117–124. https://doi.org/10.1016/j.neuro.2014.12.007

969 Puel, J.L., Pujol, R., Ladrech, S., Eybalin, M., 1991. α-Amino-3-hydroxy-5-methyl-4-isoxazole
970 propionic acid electrophysiological and neurotoxic effects in the guinea-pig cochlea.
971 Neuroscience 45, 63–72. https://doi.org/10.1016/0306-4522(91)90103-U

972 Pujol-Martí, J., López-Schier, H., 2013. Developmental and architectural principles of the lateral-
973 line neural map. Front. Neural Circuits 7, 47. https://doi.org/10.3389/fncir.2013.00047

974 Ranasinghe, P., Thorn, R.J., Seto, R., Creton, R., Bridges, W.C., Chapman, S.C., Lee, C.M.,
975 2019. Embryonic exposure to 2,2′,3,5′,6-pentachlorobiphenyl (PCB-95) causes
976 developmental malformations in zebrafish. Environ. Toxicol. Chem. 39, 162–170.
977 https://doi.org/10.1002/etc.4587

978 Ribas-Fitó, N., Sala, M., Kogevinas, M., Sunyer, J., 2001. Polychlorinated biphenyls (PCBs) and
979 neurological development in children: A systematic review. J. Epidemiol. Community
980 Health 55, 537–546. https://doi.org/10.1136/jech.55.8.537

981 Rice, D., Barone, S., 2000. Critical periods of vulnerability for the developing nervous system:
982 Evidence from humans and animal models. Environ. Health Perspect. 108, 511–533.
983 https://doi.org/10.2307/3454543

984 Roberts, A., 2000. Early functional organization of spinal neurons in developing lower
985 vertebrates. Brain Res. Bull. https://doi.org/10.1016/S0361-9230(00)00392-0

986 Rungta, R.L., Choi, H.B., Tyson, J.R., Malik, A., Dissing-Olesen, L., Lin, P.J.C., Cain, S.M.,
987 Cullis, P.R., Snutch, T.P., Macvicar, B.A., 2015. The cellular mechanisms of neuronal
988 swelling underlying cytotoxic edema. Cell 161, 610–621.
989 https://doi.org/10.1016/j.cell.2015.03.029

990 Schantz, S.L., Widholm, J.J., Rice, D.C., 2003. Effects of PCB exposure on neuropsychological
991 function in children. Environ. Health Perspect. 111, 357–576.
992 https://doi.org/10.1289/ehp.5461

993 Schindelin, J., Arganda-Carreras, I., Frise, E., Kaynig, V., Longair, M., Pietzsch, T., Preibisch,
994 S., Rueden, C., Saalfeld, S., Schmid, B., Tinevez, J.Y., White, D.J., Hartenstein, V., Eliceiri,
995 K., Tomancak, P., Cardona, A., 2012. Fiji: An open-source platform for biological-image
996 analysis. Nat. Methods 9, 676–682. https://doi.org/10.1038/nmeth.2019

997 Sebe, J.Y., Cho, S., Sheets, L., Rutherford, M.A., von Gersdorff, H., Raible, D.W., 2017. Ca^{2+}-
998 permeable AMPARs mediate glutamatergic transmission and excitotoxic damage at the
999 hair cell ribbon synapse. J. Neurosci. 37, 6162–6175.
1000 https://doi.org/10.1523/jneurosci.3644-16.2017

1001 Seegal, R.F., Bush, B., Shain, W., 1990. Lightly chlorinated ortho-substituted PCB congeners
1002 decrease dopamine in nonhuman primate brain and in tissue culture. Toxicol. Appl.
1003 Pharmacol. 106, 136–44.

1004 Serrano-Velez, J.L., Rodriguez-Alvarado, M., Torres-Vazquez, I.I., Fraser, S.E., Yasumura, T.,
1005 Vanderpool, K.G., Rash, J.E., Rosa-Molinar, E., 2014. Abundance of gap junctions at
1006 glutamatergic mixed synapses in adult Mosquitofish spinal cord neurons. Front. Neural
1007 Circuits 8, 66. https://doi.org/10.3389/fncir.2014.00066

1008 Shin, J., Park, H.-C., Topczewska, J.M., Mawdsley, D.J., Appel, B., 2003. Neural cell fate
1009 analysis in zebrafish using <i>olig2<i> BAC transgenics. Methods Cell Sci. 25, 7–14.
1010 https://doi.org/10.1023/B:MICS.0000006847.09037.3a

1011 Smith, N.L., Kimelman, D., 2019. Establishing the body plan: The first 24 hours of zebrafish
1012 development, The Zebrafish in Biomedical Research: Biology, Husbandry, Diseases, and
1013 Research Applications. Elsevier. https://doi.org/10.1016/B978-0-12-812431-4.00007-5

1014 Stenberg, M., Hamers, T., Machala, M., Fonnum, F., Stenius, U., Lauy, A.A., van Duursen,
1015 M.B.M., Westerink, R.H.S., Fernandes, E.C.A., Andersson, P.L., 2011. Multivariate toxicity
1016 profiles and QSAR modeling of non-dioxin-like PCBs - An investigation of in vitro screening
1017 data from ultra-pure congeners. Chemosphere 85, 1423–1429.
1018 https://doi.org/10.1016/j.chemosphere.2011.08.019

1019 Stewart, A.M., Braubach, O., Spitsbergen, J., Gerlai, R., Kalueff, A. V., 2014. Zebrafish models
1020 for translational neuroscience research: From tank to bedside. Trends Neurosci.
1021 https://doi.org/10.1016/j.tins.2014.02.011

1022 Ta, T.A., Feng, W., Molinski, T.F., Pessah, I.N., 2006. Hydroxylated xestospongins block
1023 inositol-1,4,5-trisphosphate-induced Ca^{2+} release and sensitize Ca^{2+}-induced Ca^{2+} release
1024 mediated by ryanodine receptors. Mol. Pharmacol. 69, 532–538.
1025 https://doi.org/10.1124/mol.105.019125.used

1026 Tabor, K.M., Bergeron, S.A., Horstick, E.J., Jordan, D.C., Aho, V., Porkka-Heiskanen, T.,
1027 Haspel, G., Burgess, H.A., 2014. Direct activation of the Mauthner cell by electric field
1028 pulses drives ultrarapid escape responses. J. Neurophysiol. 112, 834–844.
1029 https://doi.org/10.1152/jn.00228.2014

1030 Takada, N., Kucenas, S., Appel, B., 2010. Sox10 is necessary for oligodendrocyte survival
1031 following axon wrapping. Glia 58, 996–1006. https://doi.org/10.1002/glia.20981

1032 Tanaka, Y., Fujiwara, M., Shindo, A., Yin, G., Kitazawa, T., Teraoka, H., 2018. Aroclor 1254 and
1033 BDE-47 inhibit dopaminergic function manifesting as changes in locomotion behaviors in
1034 zebrafish embryos. Chemosphere 193, 1207–1215.
1035 https://doi.org/10.1016/j.chemosphere.2017.11.138

1036 Toro, C., Trapani, J.G., Pacentine, I., Maeda, R., Sheets, L., Mo, W., Nicolson, T., 2015.
1037 Dopamine modulates the activity of sensory hair cells. J. Neurosci. 35, 16494–16503.
1038 https://doi.org/10.1523/JNEUROSCI.1691-15.2015

1039 Trnovec, T., Šovčíková, E., Pavlovčinová, G., Jakubíková, J., Jusko, T.A., Hust'ák, M.,

Jurečková, D., Palkovičová, L., Kočan, A., Drobná, B., Lancz, K., Wimmerová, S., 2010. Serum PCB concentrations and cochlear function in 12-year-old children. Environ. Sci. Technol. 44, 2884–2889. https://doi.org/10.1021/es901918h

Troconis, E.L., Ordoobadi, A.J., Sommers, T.F., Aziz-Bose, R., Carter, A.R., Trapani, J.G., 2017. Intensity-dependent timing and precision of startle response latency in larval zebrafish. J. Physiol. 595, 265–282. https://doi.org/10.1113/JP272466

Tropepe, V., Sive, H.L., 2003. Can zebrafish be used as a model to study the neurodevelopmental causes of autism? Genes, Brain Behav. https://doi.org/10.1034/j.1601-183X.2003.00038.x

Vettori, M.V., Goldoni, M., Caglieri, A., Poli, D., Folesani, G., Ceccatelli, S., Mutti, A., 2006. Antagonistic effects of methyl-mercury and PCB153 on PC12 cells after a combined and simultaneous exposure. Food Chem. Toxicol. 44, 1505–1512. https://doi.org/10.1016/j.fct.2006.04.009

Voesenek, C.J., Muijres, F.T., Van Leeuwen, J.L., 2018. Biomechanics of swimming in developing larval fish. J. Exp. Biol. 221. https://doi.org/10.1242/jeb.149583

Walkowiak, J., Wiener, J.-A., Fastabend, A., Heinzow, B., Krämer, U., Schmidt, E., Steingrüber, H.-J., Wundram, S., Winneke, G., 2001. Environmental exposure to polychlorinated biphenyls and quality of the home environment: effects on psychodevelopment in early childhood. Lancet 358, 1602–1607. https://doi.org/10.1016/S0140-6736(01)06654-5

Wigestrand, M.B., Stenberg, M., Walaas, S.I., Fonnum, F., Andersson, P.L., 2013. Non-dioxin-like PCBs inhibit [3H]WIN-35,428 binding to the dopamine transporter: A structure–activity relationship study. Neurotoxicology 39, 18–24. https://doi.org/10.1016/J.NEURO.2013.07.005

Wolman, M.A., Bell, H., Hogenesch, J.B., Granato, M., Jain, R.A., Skinner, J., Hayer, K.E., Marsden, K.C., 2015. A Genome-wide Screen Identifies PAPP-AA-Mediated IGFR Signaling as a Novel Regulator of Habituation Learning. Neuron 85, 1200–1211. https://doi.org/10.1016/j.neuron.2015.02.025

Yang, D., Kim, K.H., Phimister, A., Bachstetter, A.D., Ward, T.R., Stackman, R.W., Mervis, R.F., Wisniewski, A.B., Klein, S.L., Kodavanti, P.R.S., Anderson, K.A., Wayman, G., Pessah, I.N., Lein, P.J., 2009. Developmental exposure to polychlorinated biphenyls interferes with experience-dependent dendritic plasticity and ryanodine receptor expression in weanling rats. Environ. Health Perspect. 117, 426–435. https://doi.org/10.1289/ehp.11771

Zhao, Y., Liang, J., Meng, H., Yin, Y., Zhen, H., Zheng, X., Shi, H., Wu, X., Zu, Y., Wang, B., Fan, L., Zhang, K., 2020. Rare earth elements lanthanum and praseodymium adversely affect neural and cardiovascular eevelopment in zebrafish (Danio rerio). Environ. Sci. Technol. https://doi.org/10.1021/acs.est.0c06632